

---

Electronic Thesis and Dissertation Repository

---

6-6-2019 10:30 AM

## Effect of the nonlinear material viscosity on the performance of dielectric elastomer transducers

Yuanping Li  
*The University of Western Ontario*

Supervisor  
Jiang, Liying  
*The University of Western Ontario*

Graduate Program in Mechanical and Materials Engineering  
A thesis submitted in partial fulfillment of the requirements for the degree in Master of Engineering Science  
© Yuanping Li 2019

Follow this and additional works at: <https://ir.lib.uwo.ca/etd>



Part of the [Applied Mechanics Commons](#), [Computer-Aided Engineering and Design Commons](#), [Electro-Mechanical Systems Commons](#), [Energy Systems Commons](#), [Engineering Mechanics Commons](#), [Mechanics of Materials Commons](#), [Polymer and Organic Materials Commons](#), and the [Semiconductor and Optical Materials Commons](#)

---

### Recommended Citation

Li, Yuanping, "Effect of the nonlinear material viscosity on the performance of dielectric elastomer transducers" (2019). *Electronic Thesis and Dissertation Repository*. 6223.  
<https://ir.lib.uwo.ca/etd/6223>

This Dissertation/Thesis is brought to you for free and open access by Scholarship@Western. It has been accepted for inclusion in Electronic Thesis and Dissertation Repository by an authorized administrator of Scholarship@Western. For more information, please contact [wlsadmin@uwo.ca](mailto:wlsadmin@uwo.ca).

# Abstract

As a typical type of soft electroactive materials, dielectric elastomers (DEs) are capable of producing large voltage-induced deformation, which makes them desirable materials for a variety of applications in transduction technology, including tunable oscillators, resonators, biomimetics and energy harvesters. The dynamic and energy harvesting performance of such DE-based devices is strongly affected not only by multiple failure modes such as electrical breakdown, electromechanical instability, loss-of-tension and fatigue, but also by their material viscoelasticity. Moreover, as suggested by experiments and theoretical studies, DEs possess nonlinear relaxation processes, which makes modeling of the performance of DE-based devices more challenging.

In this thesis, by adopting the state-of-art modeling framework of finite-deformation viscoelasticity, the effects of nonlinear viscosity of the polymer chains on the oscillation and frequency tuning of DE membrane oscillators are firstly investigated. From the simulation results, it is found that the nonlinear viscosity only affects the transient state of the frequency tuning process of DE oscillators. Secondly, with both finite-deformation viscoelasticity and deformation-dependent viscosity of polymer chains considered, the energy conversion efficiency and the harvested energy of dielectric elastomer generators under equi-biaxial loading are also examined. It is found that when a nonlinear viscosity model is used, DE generators appear to reach an equilibrium state faster and the nonlinear viscosity significantly influences the energy harvesting performance. The modeling framework developed in this work is expected to provide useful guidelines for predicting the performance of DE-based oscillators and energy harvesters as well as their optimal design.

## Keywords

Dielectric elastomers transducers, viscoelasticity, nonlinear viscosity, hyperelasticity, electrical breakdown, frequency tuning, energy harvesting.

## Acknowledgments

I would like to express my great sincere gratitude to my supervisor Prof. Liying Jiang for providing this graduate study opportunity and patiently guiding me. I would also like to thank my advisory committee members Dr. Price and Dr. Khayat for their valuable advices on this project. Thank Dr. Jianyou Zhou for thesis revision and guidance, also thank my colleagues Asim, Xiaotian, Liyang and Mohammad for helping and supporting.

# Table of Contents

Abstract.....	i
Acknowledgments.....	ii
List of Figures.....	v
Nomenclature.....	viii
Chapter 1.....	1
1 Introduction.....	1
1.1 Dielectric elastomers and applications.....	1
1.2 Large deformation capacity and typical electromechanical responses of dielectric elastomers .....	4
1.3 Viscoelastic behavior of dielectric elastomers.....	6
1.4 Objective.....	8
1.5 Thesis structure.....	8
Chapter 2.....	9
2 Literature review .....	9
2.1 Fully coupled field theory.....	9
2.2 Finite-deformation viscoelastic theory .....	14
2.3 Finite-deformation viscoelasticity of elastomers with nonlinear viscosity.....	17
Chapter 3.....	19
3 Investigation on dynamic performance of viscoelastic dielectric elastomer oscillator considering material nonlinear viscosity.....	19
3.1 Introduction.....	19
3.2 Models and formulations .....	21
3.3 Resonant frequency of an oscillator.....	29
3.4 Forced response of an oscillator .....	39
3.5 Conclusion .....	43

Chapter 4.....	44
4 The effect of nonlinear viscosity on the performance of dielectric elastomer energy generators .....	44
4.1 Introduction.....	44
4.2 Model and Formulation.....	47
4.3 Energy harvesting cycle of DEGs.....	53
4.4 Conclusion .....	64
Chapter 5.....	65
5 Conclusion and future work.....	65
5.1 Contribution .....	65
5.2 Conclusion remarks .....	66
5.3 Future work.....	66
References.....	68
Curriculum Vitae .....	75

## List of Figures

Figure 1-1 A dielectric elastomer membrane sandwiched by two compliant electrodes (a) undeformed state (b) current state.....	1
Figure 1-2 "FLEX", an insect shape walking robot with dielectric elastomer actuators (Pelrine et al., 2002). .....	3
Figure 1-3 Dielectric elastomers are used in loudspeakers (a) Three acrylic diaphragm speakers. The larger speaker is 12in × 12in (b) Frequency response of a speaker made from silicon film on a matrix of holes (inset) (Kornbluh et al., 2002). .....	3
Figure 1-4 Dielectric electric generator system used to harvest energy from ocean waves (Chiba et al., 2008).....	4
Figure 1-5 Electromechanical response and electrical breakdown of dielectric elastomers. (a)-(c) Three types behavior are defined (Koh et al., 2011b). .....	5
Figure 2-1 A dielectric body subjected to electromechanical loads in the current state.....	10
Figure 2-2 Rheological model for viscoelastic DEs. ....	14
Figure 2-3 Schematic of a polymer chain constrained in a tube region with primitive chain C-D (a) polymer chain end C and D crosslinked with other chains; (b) the polymer chain entangles with other polymer chains at C and D. (Zhou et al., 2018) .....	18
Figure 3-1 Schematic of a DE membrane oscillator (a) undeformed state; (b) pre-stretched state; (c) current state .....	23
Figure 3-2 Illustration of a polymer chain confined in a tube-like region with the tube diameter of $a$ . (a) Polymer chain A-B is represented by its primitive chain (blue color); (b) dimensions of the primitive chain.....	29
Figure 3-3 Variation of stretch ratio with time for two different viscosity models when a static voltage is applied. (a) Time interval is from 9.5 s to 11 s; (b) time interval is from 0 s to 60 s.....	33

Figure 3-4 Frequency tuning process for two different viscosity models when a static voltage is applied. (a) Time interval is from 9.5 s to 11 s; (b) time interval is from 0 s to 60 s.....	34
Figure 3-5 Effect of loading rate of the applied voltage ( $dV^* / dt = 1$ ) on frequency tuning for two different viscosity models. (a) Time interval is from 9.5 s to 11 s; (b) time interval is from 0 s to 60 s.....	36
Figure 3-6 Effect of loading rate of the applied voltage ( $dV^* / dt = 0.1667$ ) on frequency tuning for two different viscosity models. (a) Time interval is from 9.5 s to 11 s; (b) time interval is from 0 s to 60 s.....	37
Figure 3-7 Variation of the tuned frequency for purely elastic and viscoelastic DE resonators within a certain range of applied voltage.....	38
Figure 3-8 Variation of the stretch ratio with time (0s to 60s) for two different viscosity models when an AC voltage is applied.....	39
Figure 3-9 Representation model of external excitation applied on an oscillator's frame .....	40
Figure 3-10 Time response of the DE membrane oscillator under external excitation. The excitation frequency $\omega_b$ varies between $0.01\omega_n$ ((a) and (b)) and $1.5\omega_n$ ((c) and (d)). The amplitude of excitation $Y$ varies between $0.01L_1$ ((a) and (c)) and $1L_1$ ((b) and (d)).....	42
Figure 4-1 Schematics of a dielectric elastomer membrane embedded in a DEG. (a) reference state (b) current state with voltage $\Phi$ and pre-stretch force $P$ applied.....	48
Figure 4-2 (a) A tube-like region confines polymer chain C-D. The axis of the tube is the primitive chain of polymer chain C-D; (b) description of the primitive chain.....	53
Figure 4-3 Energy harvesting cycle of the DEG: (a) proposed triangular path, experimental path, simulation results by using both nonlinear and linear viscosity models; (b) circuit diagram used to control harvesting cycle.....	56
Figure 4-4 The force-stretch curve of the DE membrane during the electromechanical harvesting cycle for different viscosity models.....	58

Figure 4-5 The variation of charge (a), voltage (b) and current leakage (c) on the DE capacitor during the electromechanical harvesting cycle. .... 59

Figure 4-6 Variation of harvested energy and efficiency DEG with the stretch ratio at  $C_3$  and the voltage level of power supply (a) harvesting energy (b) conversion efficiency. .... 61

Figure 4-7 Maximum harvested energy (a) and maximum efficiency (b) of DE in terms of material parameter  $\chi$ . .... 63



# Nomenclature

$\Phi$	voltage
$\Phi_B$	electrical breakdown voltage
$\lambda$	equi-biaxial stretch ratio
$\varepsilon$	relative dielectric constant
$\varepsilon_0$	dielectric permittivity of vacuum
$E$	electric field
$V_0$	volume in reference state
$\mathbf{b}$	body force
$\mathbf{T}$	traction force
$\boldsymbol{\sigma}$	true stress
$\mathbf{E}$	true electric field
$\mathbf{S}$	nominal stress
$\tilde{\mathbf{E}}$	nominal electric field
$W^{EQ}$	equilibrium Helmholtz free energy density
$W^{NEQ}$	non-equilibrium Helmholtz free energy density
$w$	Helmholtz free energy density
$G$	total free energy
$\mathbf{F}$	deformation gradient

$\mathbf{F}^e$	elastic deformation gradient
$\mathbf{F}^i$	inelastic deformation gradient
$\eta$	viscosity in current state
$\eta_0$	viscosity in reference state
$\zeta$	monomer friction constant
$N$	polymerization degree of chains
$b_0$	effective bond length between monomers
$G_0$	shear relaxation modulus
$T$	temperature
$k_B$	Boltzmann constant
$a$	tube diameter
$L$	primitive chain length
$\mathbf{R}$	end to end vector of primitive chain in reference state
$f_0(\mathbf{R})$	statistical distribution function of end to end vector in reference state
$\mathbf{u}$	unit tangent vector in reference state
$G^{EQ}$	equilibrium shear modulus
$G^{NEQ}$	non-equilibrium shear modulus
$\chi$	fraction of the time independent polymer
$\mathbf{I}$	second order identity tensor

$\mathbf{I}^4$	fourth order symmetric identity tensor
$\gamma^{-1}$	isotropic rank-four mobility tensor
$\omega_n$	natural frequency
$V^*$	dimensionless voltage
$\omega_b$	excitation frequency
$Y$	excitation amplitude
$C_{DE}$	capacitance of DE
$\Phi_L$	voltage of power supply

## Chapter 1

### 1 Introduction

#### 1.1 Dielectric elastomers and applications

Dielectric elastomers (DEs) consist of randomly oriented dipoles that respond to electrical stimuli. When a dielectric elastomer is subjected to an electric field, the dipoles within the material tend to align themselves along the electric field. This unique property of dielectric elastomers makes them desirable materials for energy transducers. Figure 1-1 illustrates the basic element of a dielectric elastomer transducer. Figure 1-1 (a) shows a membrane of undeformed dielectric elastomer membrane sandwiched between two compliant electrodes. In figure 1-1 (b), a voltage is applied on the electrodes and opposite charges flow from external power supply to the compliant electrodes. The attractive force between the charges on the electrodes makes the DE membrane contract in thickness and expand in area to the current state (Hong, 2011; Suo, 2010; Zhao and Suo, 2010).

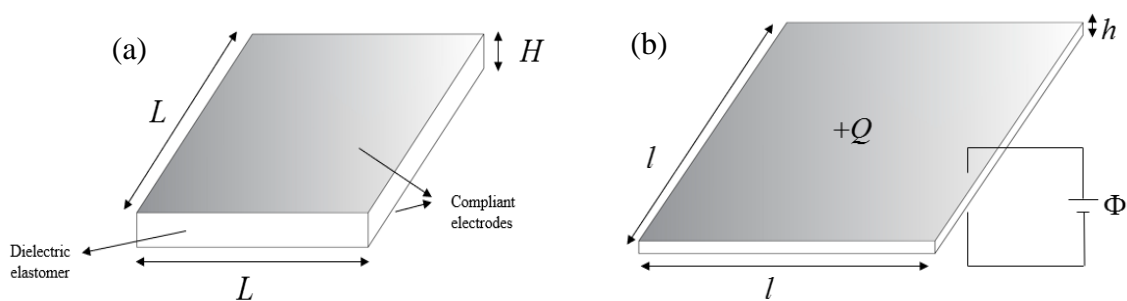


**Figure 1-1 A dielectric elastomer membrane sandwiched by two compliant electrodes (a) undeformed state (b) current state**

Decades ago, it was found that dielectric elastomers possessed great potential for sustaining large deformation with strain over 100% (Pelrine et al., 2000). Due to large deformation capability, high energy density, softness and flexibility, DEs are excellent material candidates for actuators, sensors, oscillators and energy harvesters (Suo, 2010). For example, in figure 1-2, an insect-inspired walking robot is designed by using two linear

dielectric elastomer actuators on each leg. The advantage of DEs in this application is that they avoid gears and provide flexible movements (Kornbluh et al., 2002; Pelrine et al., 2002). Also, due to their comparable softness as human tissue, dielectric elastomer actuators have the ability to be implemented as artificial muscles or organs in robotics and bioengineering field (Ashley, 2003). For example, an artificial human heart with contraction and expansion to ensure flow of blood; an eardrum to convert mechanical motion into acoustic signals; artificial pupils capable of adjusting in response to light intensity (Pelrine et al., 2002). Also, compared to traditional sensor materials which are relatively stiff, DE sensors are adaptable and capable of sustaining large strain. For example, a Japanese company EAMEX has claimed to have conducted a DE sensor being able to sense external forces (Jung et al., 2008). Goulbourne et al. (2007) proposed a self-sensing McKibben actuator which utilized a DE cylindrical capacitive sensor to define the change in strain and pressure of the McKibben pneumatic actuator.

DEs have also been developed and explored for applications as loudspeaker, oscillators and resonators. Figure 1-3 illustrates the design of dielectric elastomer speakers. Dielectric elastomer speakers have many advantages, including various shapes (e.g. conformal, flat, round), good fidelity, high sensitivity, and consistent sound pressure response over a wide range of frequency (Kornbluh et al., 2002). Furthermore, DEs have shown potential for energy harvesting devices or generators which can harvest energy from a variety of sources, such as wind, ocean waves, and human movements (Chiba et al., 2008; Kornbluh et al., 2012; Pelrine et al., 2001). Figure 1-4 demonstrates a dielectric elastomer generator designed to harvest mechanical energy from ocean waves. Experimental results show that it can produce a peak power of 11W and attain an energy density up to 80J/kg (Chiba et al., 2008).

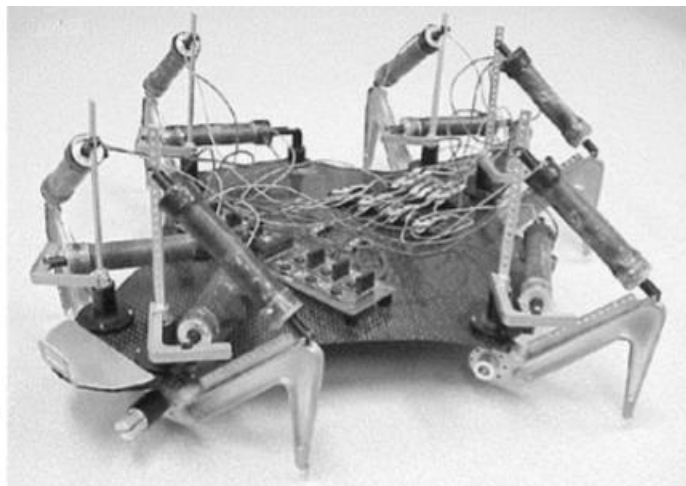


**Figure 1-2 "FLEX", an insect shape walking robot with dielectric elastomer actuators (Pelrine et al., 2002).**

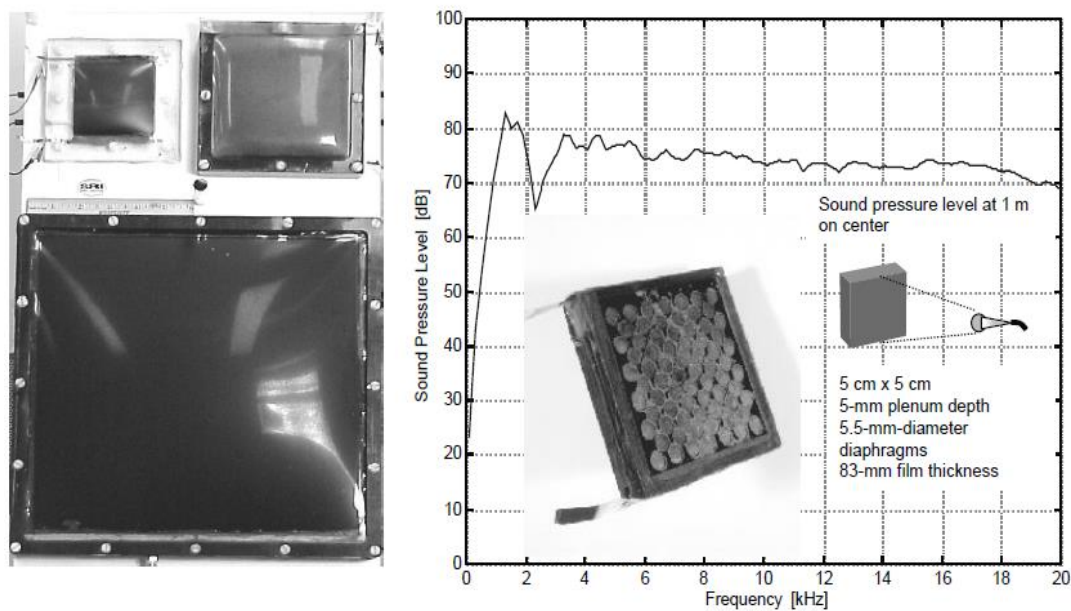


**Figure 1-3 Dielectric elastomers are used in loudspeakers (a) Three acrylic diaphragm speakers. The larger speaker is 12in  $\times$  12in (b) Frequency response of a speaker made from silicon film on a matrix of holes (inset) (Kornbluh et al., 2002).**

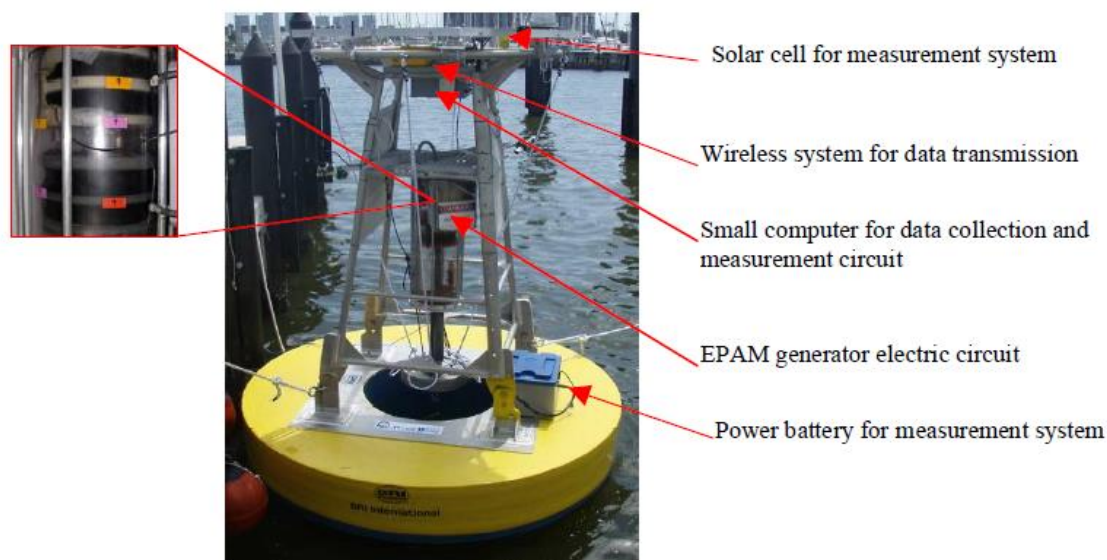


**Figure 1-4 Dielectric electric generator system used to harvest energy from ocean waves (Chiba et al., 2008).**

## 1.2 Large deformation capacity and typical electromechanical responses of dielectric elastomers

Dielectric materials deform when subjected to a voltage, but the amount of deformation varies significantly. For instance, piezoelectric ceramics can only attain strains less than 1%; glass and semi-crystalline polymers can attain strains up to 10% (Zhang et al., 1998). For dielectric elastomers, actuation strains over 100% have been achieved by a few approaches, for example, by applying pre-stretch (Pelrine et al., 2000), using interpenetrating networks (Ha et al., 2006), swelling an elastomer with a solvent (Shankar et al., 2007), and spraying charges on compliant electrodes (Keplinger et al., 2010). However, existing studies have also found that the voltage-induced deformation of DEs is strongly affected by multiple failure modes and electromechanical instability (EMI). Among the failure modes of DEs, electrical breakdown is the most common one, which occurs when the applied voltage exceeds the breakdown voltage of the material. Electromechanical instability is a phenomenon when the applied voltage increases, the elastomer thins down, and the same voltage induces an even higher electric field, which

causes the elastomer to reduce the thickness dramatically and eventually results in a premature electrical breakdown (Keplinger et al., 2012; Suo, 2010).

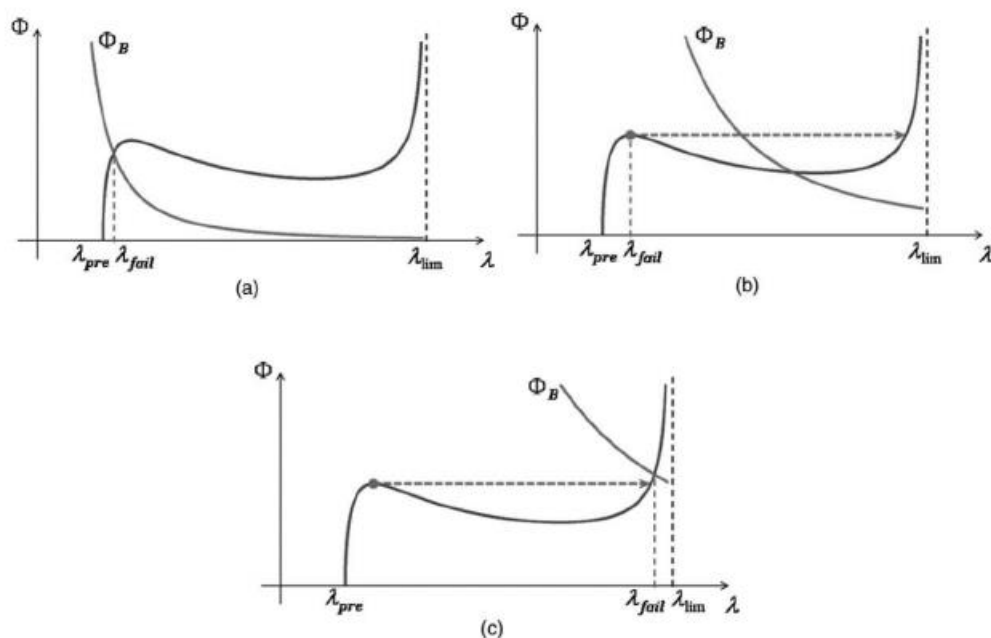


**Figure 1-5 Electromechanical response and electrical breakdown of dielectric elastomers. (a)-(c) Three types behavior are defined (Koh et al., 2011b).**

Based on the interplay among the electrical breakdown, the electromechanical instability, and the electromechanical response, dielectric elastomers can be classified into three types as demonstrated by Figure 1-5, in which both the electromechanical response curve and the electrical breakdown curve are plotted. In figure 1-5 (a), the electrical breakdown happens before the peak of the response curve. For this case, the actuation of the DE fails by the electrical breakdown. In figure 1-5 (b), due to the electromechanical instability, the electrical breakdown happens during the snap-through deformation, where the DE fails by a premature electrical breakdown. In figure 1-5 (c), the electrical breakdown happens after the snap-through deformation and large deformation of the DE is achieved (Leng et al., 2009). In other words, DEs with low dielectric strength (figure 1-5 (a)) do not undergo EMI. For DEs with moderate dielectric strength (figure 1-5 (b)), EMI occurs during the actuation and DE fails by a premature electrical breakdown. For DEs with high



dielectric strength (figure 1-5 (c)), the actuation survives the EMI and results in large deformation (Koh et al., 2011b; Zhao and Suo, 2010).

### 1.3 Viscoelastic behavior of dielectric elastomers

It has been found in experiments that the electromechanical response of DEs is also highly rate-dependent (Löwe et al., 2005; Pelrine et al., 2000; Plante and Dubowsky, 2006), which is caused by the intrinsic material viscosity of DEs. The rate-dependency of DEs can strongly affect its dynamic performance and coupling efficiency (Kornbluh et al., 2000). To predict their dynamic performance and improve the performance of various DE-based vibrational devices, researchers have devoted much effort to modeling viscoelastic DEs. In the early studies, a nonlinear viscoelastic model for DE membrane was developed using the Christensen's theory (Christensen, 1980) of viscoelasticity for small and large deformation (Yang et al., 2005). A quasi-linear viscoelasticity model with time-dependent coefficients was implemented to describe the nonlinear response of circular DE membranes (Wissler and Mazza, 2005). Later, the material viscoelasticity of DEs was studied with a modified hyperelastic model (Plante and Dubowsky, 2007). Recently, based on the fully coupled field theory (Suo et al., 2008) and the finite-deformation viscoelasticity theory (Reese and Govindjee, 1998), a constitutive model was developed by Hong (2011), which is capable of adopting most hyperelastic energy functions and thermodynamic evolution laws. With this constitutive model for DEs, Park and Nguyen developed a finite-deformation finite element model and evaluated the viscoelastic response of DEs undergoing homogeneous deformation and the effects of shear and bulk relaxation time on the EMI phenomenon (Park and Nguyen, 2013). Zhang et al. (2015b) presented a theoretical prediction on the dynamic behavior of viscoelastic DE membranes subjected to three different loads: equal-biaxial, uni-axial, and pure shear forces. Later, Wang et al. (2013) analyzed the inhomogeneous viscoelastic deformation of a DE subjected to a combination of pressure and voltage.

Moreover, it has been confirmed that the time-dependent inelastic deformation and stress relaxation significantly affect the dynamic response of DEs (Chiang Foo et al., 2012a). Recently, more studies have been conducted to investigate the performance of

viscoelastic DE resonators and oscillators. Zhou et al. (2014) investigated the frequency tuning process of a viscoelastic DE-based resonator. Zhang et al. (2015a) developed an analytical model to investigate the coupled nonlinear oscillation and the stability of viscoelastic dielectric elastomers under non-equiaxial forces. Zhou et al. (2016) investigated the frequency tuning of a viscoelastic DE membrane oscillator, as well as its response to external excitation and AC voltage.

DE generators are another typical application of DEs that are strongly affected by the material viscoelasticity (Huang et al., 2013; Pelrine et al., 2001; Shian et al., 2014). Foo et al. (2012b) investigated the effect of material viscoelasticity and current leakage on dielectric elastomer generators. Li et al. (2012b) demonstrated an approach to characterize the energy harvesting performance of viscoelastic DE generators under inhomogeneous fields. Zhou et al. (2017) presented a theoretical framework for analyzing the energy conversion performance of DEGs using a triangular harvesting scheme with the consideration of various failure modes.

From the above-mentioned studies, much effort has been devoted to investigating the actuation, dynamic performance, failure modes and energy harvesting performance of viscoelastic dielectric elastomer-based oscillators or generators. However, much less work has been focused on the effect of deformation-dependent viscosity. When large deformation is considered, a more realistic situation is that the viscosity of the polymer chain is deformation-dependent, which has also been confirmed by experiments (Pyckhout-Hintzen et al., 2013; Straube et al., 1995). The nonlinear viscosity of material can be explained by the tube model proposed by Doi and Edwards (Doi and Edwards, 1988). In the theory by Doi and Edwards (Doi and Edwards, 1988), a tube-like region surrounding a polymer chain restricts its lateral motion, but allows the chain to move back and forth or reptate within the tube. When the elastomer is under large deformation, the diameter of this tube-like region changes, which could significantly affect the reptation and relaxation ability of the polymer chain (Doi and Edwards, 1988). This deformation-dependency of viscosity may also strongly influence the dynamic behavior and electromechanical coupling of DEs.

## 1.4 Objective

As discussed above, dielectric elastomers have demonstrated great potential in various applications due to their unique features like high energy density, flexibility and capability of large deformation. However, due to the complex interplay among electromechanical coupling, material viscoelasticity and various failure modes, it is still difficult to predict the dynamic performance of DEs. Moreover, most of the existing works do not consider the deformation-dependent viscosity of dielectric elastomers, which may also strongly affect the dynamic and energy harvesting performance of DEs. Therefore, the objective of this work is to develop robust models for predicting the dynamic and the energy harvesting performance of DE-based devices as well as provide guidelines for their optimal design. Details are given as follows:

- (1) Examining the effect of nonlinear viscosity on the frequency tuning process of viscoelastic DE oscillators and resonators as well as their performance under external excitation.
- (2) Investigating the effect of deformation-dependent viscosity on the energy harvesting efficiency and the energy density of DE-based generators.

## 1.5 Thesis structure

Following the general introduction and objectives in chapter 1, a literature review about the fully coupled field theory, the viscoelastic models, as well as the finite-deformation viscoelasticity theory for elastomers with nonlinear viscosity is given in chapter 2. In chapter 3, the effect of the deformation-dependent material viscosity on the frequency tuning of viscoelastic DE based resonators, as well as their behavior under external excitation are investigated. In chapter 4, the nonlinear viscosity is further incorporated into the finite-deformation viscoelasticity theory to study energy harvesting performance of dielectric generators. MATLAB codes are developed in both Chapter 3 and Chapter 4 for numerical simulations. Chapter 5 summarizes this thesis and provides recommendations for future work.

## Chapter 2

### 2 Literature review

Over recent decades, dielectric elastomers have drawn much attention due to their wide range of applications like artificial muscles, energy harvesters, medical and biomimetic equipment. Extensive studies have been carried out to analyze the interplay of their electromechanical deformation, failure modes and material viscoelasticity. The following section presents a review of the relevant studies on modelling the complex electromechanical coupling behavior of DEs.

#### 2.1 Fully coupled field theory

Early analyses on DEs tended to consider the material as linear elastic by neglecting the effect of large deformation, and modeled the electromechanical coupling by simply adding the Maxwell stress (Kornbluh et al., 1995; Pelrine et al., 1998). However, since the relation between strain and stress is assumed to be linear, the analyses are limited to small deformation. In order to account for finite-deformation, researchers later implemented the hyperelastic constitutive laws into a uniformly deformed elastomer, and have achieved results that are in agreement with some experimental observations (Goulbourne et al., 2005; Pelrine et al., 2000; Wissler and Mazza, 2005). Nevertheless, these uncoupled models are only capable of explaining certain experimental results. Later, a fully coupled nonlinear field theory for electromechanical response of DEs was proposed to model the deformation and instability of dielectric elastomers (Dorfmann and Ogden, 2005; McMeeking and Landis, 2005). This fully coupled field theory is capable of explaining the nonlinear electromechanical response of DEs and enabling further numerical simulations of dielectric elastomers under complex loading conditions. The fully coupled field theory (McMeeking and Landis, 2005; Suo et al., 2008) is elaborated as follows.

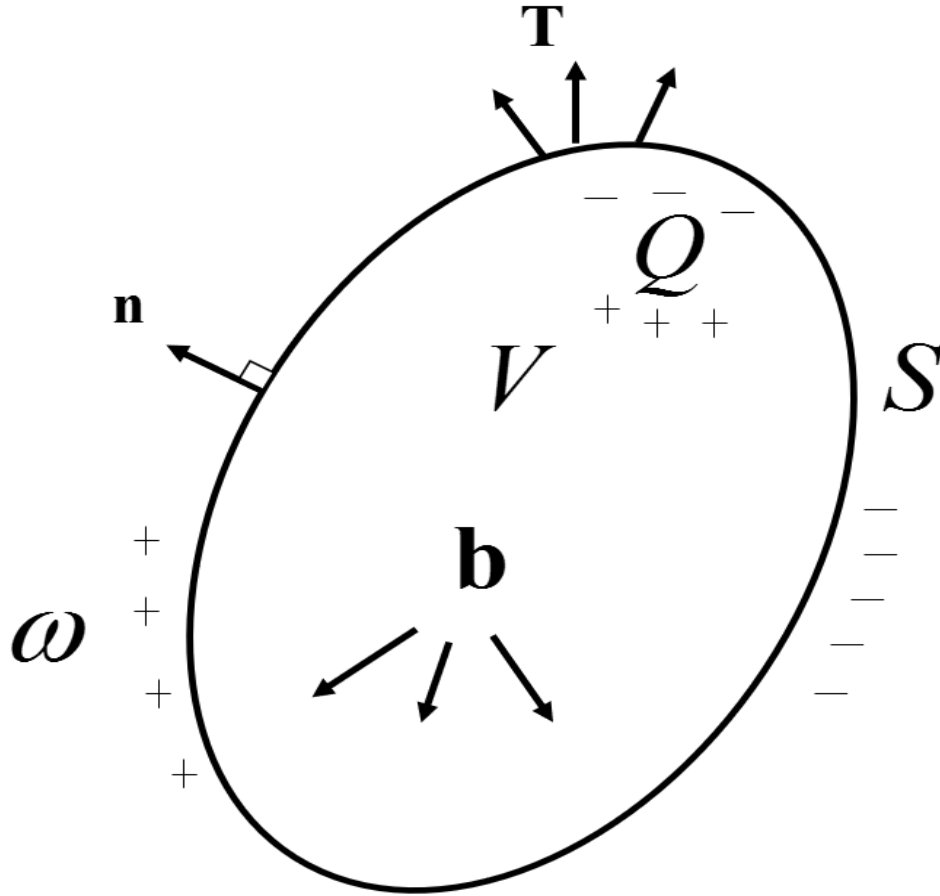


**Figure 2-1 A dielectric body subjected to electromechanical loads in the current state**

Figure 2-1 shows a dielectric body which is subjected to free body charge  $Q(\mathbf{X}, t)$ , free surface charge  $\omega(\mathbf{X}, t)$ , body force  $\mathbf{b}(\mathbf{X}, t)$ , and surface traction  $\mathbf{T}(\mathbf{X}, t)$ . Under these loads, a material point in the dielectric body moves from the reference position  $\mathbf{X}$  to the current position  $\mathbf{x}(\mathbf{X}, t)$  at time  $t$ . The dielectric body has an initial volume of  $V_0$ , mass density of  $\rho$  and surface area of  $S_0$ . The deformation gradient of the current state with respect to the reference state is defined as

$$F_{ik} = \frac{\partial x_i(\mathbf{X}, t)}{\partial X_k}. \quad (2.1)$$

Consider any test function  $\xi_i(\mathbf{X})$ ,

$$\int_{V_0} \frac{\partial \xi_i}{\partial X_k} s_{ik} dV_0 = \int_{S_0} T_i \xi_i dS_0 - \int_{V_0} \xi_i \frac{\partial s_{ik}}{\partial X_k} dV_0, \quad (2.2)$$

where  $s_{ik}$  is the Piola-Kirchhoff stress (nominal stress). The motion equation of the dielectric body is expressed as

$$\frac{\partial s_{ik}}{\partial X_k} = -b_i + \rho \frac{d^2 x_i}{dt^2}. \quad (2.3)$$

Combining equations (2.2) and (2.3) we obtain

$$\int_{V_0} \frac{\partial \xi_i}{\partial X_k} s_{ik} dV_0 = \int_{S_0} T_i \xi_i dS_0 + \int_{V_0} \xi_i b_i dV_0 - \int_{V_0} \rho \frac{d^2 x_i}{dt^2} \xi_i dV_0. \quad (2.4)$$

Again, consider any test function  $\eta(X)$ ,

$$\int_{V_0} \frac{\partial \eta}{\partial X_k} \tilde{D}_k dV_0 = - \int_S \omega \eta dS - \int_{V_0} \eta \frac{\partial \tilde{D}_k}{\partial X_k} dV_0, \quad (2.5)$$

where  $\tilde{D}_k$  is nominal electric displacement, and  $\tilde{E}_k$  is nominal electric field which could be expressed in terms of the electric potential,

$$\tilde{E}_k = - \frac{\partial \Phi}{\partial X_k}. \quad (2.6)$$

According to Maxwell's law and Gauss' law, the divergence of the electric displacement is equal to the free charge per unit volume, i.e.,

$$\frac{\partial \tilde{D}_k}{\partial X_k} = Q. \quad (2.7)$$

Combining equations (2.5) and (2.7) results in,

$$\int_{V_0} \frac{\partial \eta}{\partial X_k} \tilde{D}_k dV_0 = - \int_{S_0} \omega \eta dS_0 - \int_{V_0} \eta Q dV_0, \quad (2.8)$$

which holds true for any arbitrary test function  $\eta(X)$ .

For any small changes on deformation and electric charge, the corresponding small change of the free energy of the system is expressed as,

$$\begin{aligned} \delta G = & \int_{V_0} \delta W dV - \int_V b_i \delta x_i dV - \int_S T_i \delta x_i dS - \int_V \delta Q \Phi dV \\ & - \int_S \delta \omega \Phi dS + \int_V \rho \frac{d^2 x_i}{dt^2} \delta x_i dV \end{aligned}, \quad (2.9)$$

Combining equations (2.4), (2.8) and (2.9), it becomes

$$\delta G = \int_{V_0} \left( \delta W - \delta F_{ik} s_{ik} - \tilde{E}_k \delta \tilde{D}_k \right) dV_0. \quad (2.10)$$

Moreover, for purely elastic elastomers,

$$\delta W = \frac{\partial W}{\partial F_{ik}} \delta F_{ik} + \frac{\partial W}{\partial \tilde{D}_k} \delta \tilde{D}_k. \quad (2.11)$$

Then the change of the free energy density of the system is further expressed as,

$$\delta G = \int_{V_0} \left( \frac{\partial W}{\partial F_{ik}} - s_{ik} \right) \delta F_{ik} dV_0 + \int_{V_0} \left( \frac{\partial W}{\partial \tilde{D}_k} - \tilde{E}_k \right) \delta \tilde{D}_k dV_0. \quad (2.12)$$

Thus, the constitutive equations according to the coupled field theory are determined as,

$$s_{ik} = \frac{\partial W(\mathbf{F}, \tilde{\mathbf{D}})}{\partial F_{ik}}, \quad (2.13)$$

$$\tilde{E}_k = \frac{\partial W(\mathbf{F}, \tilde{\mathbf{D}})}{\partial \tilde{D}_k}, \quad (2.14)$$

Then the true stress  $\boldsymbol{\sigma}$ , the true electric displacement and the true electric field  $\mathbf{E}$  are further determined in terms of the nominal quantities, i.e.,

$$\sigma_{ij} = \frac{s_{ik} F_{jk}}{\det \mathbf{F}}, \quad (2.15)$$

$$D_i = \frac{\tilde{D}_k F_{ik}}{\det \mathbf{F}}, \quad (2.16)$$

$$E_i = F_{ik}^{-1} \tilde{E}_k. \quad (2.17)$$

Also, experiments suggest that,

$$D_i = \varepsilon \varepsilon_0 E_i, \quad (2.18)$$

where  $\varepsilon_0$  is the dielectric permittivity of vacuum,  $\varepsilon$  is the relative dielectric constant of the dielectric medium. The framework of nonlinear fully coupled field theory has been extensively adopted in the literature to further study the electromechanical coupling of dielectric elastomers under complex working conditions. For example, Zhao and Suo (2007) analyzed the electromechanical stability of DE actuators. Huang and Suo (2011) investigated the electromechanical phase transition of DEs.



## 2.2 Finite-deformation viscoelastic theory

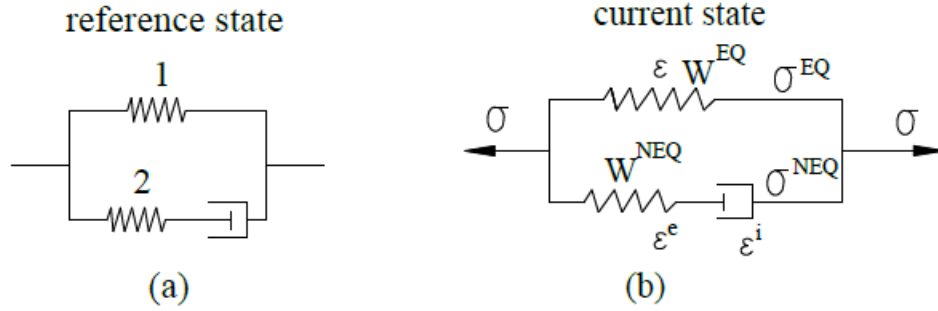


**Figure 2-2 Rheological model for viscoelastic DEs.**

As mentioned above, DE exhibits viscoelastic properties. Figure 2.2 shows the rheological model to represent the viscoelasticity of DEs. As treated in the work of Lee (Lee, 1969) and Hong (Hong, 2011), the total deformation can be multiplicatively decomposed into an elastic part and an inelastic part as,

$$\mathbf{F}_{ik} = \mathbf{F}_{im}^e \mathbf{F}_{mk}^i, \quad (2.19)$$

where the superscripts ‘e’ and ‘i’ represent elastic and inelastic components, respectively. With the consideration of viscoelasticity, the Helmholtz free energy density is not only a function of the total deformation and the electric displacement. As shown in figure 2-2, the total Helmholtz free energy density of the system consists of two parts: one is the equilibrium Helmholtz free energy  $W^{EQ}(\mathbf{F}, \tilde{\mathbf{D}})$  and the other is the non-equilibrium Helmholtz free energy  $W^{NEQ}(\mathbf{F}^e)$ .  $W^{EQ}$  is stored in the “time infinity” spring and  $W^{NEQ}$  is the strain energy in the Maxwell element. The dashpot relaxes with time and results in energy dissipation (Lee, 1969; Reese and Govindjee, 1998). Since the electric field equilibrates much faster than the mechanical field, it can be assumed that the electric field is always in equilibrium, i.e.,  $\tilde{\mathbf{E}} \equiv \tilde{\mathbf{E}}^{EQ}$ . Furthermore, the equilibrium Helmholtz free energy density is equal to the sum of the strain energy density  $W_s(\mathbf{F})$  and the polarization energy (Zhao et al., 2007), i.e.,

$$W^{\text{EQ}}(\mathbf{F}, \tilde{\mathbf{D}}) = W_s(\mathbf{F}) + \frac{F_{ij}F_{ik}}{2\varepsilon\varepsilon_0 \det(\mathbf{F})} \tilde{D}_i \tilde{D}_k. \quad (2.20)$$

Therefore, the variation of the strain energy density function is expressed as,

$$\delta W = \frac{\partial W}{\partial F_{ik}} \delta F_{ik} + \frac{\partial W}{\partial F_{mk}^i} \delta F_{mk}^i + \frac{\partial W}{\partial \tilde{D}_k} \delta \tilde{D}_k. \quad (2.21)$$

The second law of thermodynamics suggests that the free energy of the system never increases, i.e.,  $\delta G \leq 0$ . This inequality must hold true in any volume. Therefore,

$$\delta W - \delta F_{ik} s_{ik} - \tilde{E}_k \delta \tilde{D}_k \leq 0. \quad (2.22)$$

Combining equations (2.21) and (2.22) results in,

$$\frac{\partial W}{\partial F_{ik}} \delta F_{ik} - s_{ik} \delta F_{ik} + \frac{\partial W}{\partial F_{mk}^i} \delta F_{mk}^i \leq 0. \quad (2.23)$$

For an arbitrary variation of the dielectric elastomer body, the variation in the free energy of the body regarding to the change of the deformation gradient is equal to the work done by the external force (Coleman and Gurtin, 1967), which gives

$$\frac{\partial W}{\partial F_{ik}} \delta F_{ik} - s_{ik} \delta F_{ik} = 0. \quad (2.24)$$

Thus, only the inelastic term in inequality (2.23) retains, i.e.,

$$s_{ik}^{\text{NEQ}} F_{im}^e H_{nk}^i \delta F_{mn}^i \geq 0, \quad (2.25)$$

where the inelastic first Piola-Kirchhoff stress tensor  $s_{ik}^{\text{NEQ}}$  is given by

$$s_{ik}^{NEQ} = \frac{\partial W^{NEQ}}{\partial F_{ik}^e}, \quad (2.26)$$

Accordingly, the inelastic Cauchy stress tensor can be expressed as,

$$\sigma_{ij}^{NEQ} = \frac{s_{ik}^{NEQ} F_{jk}^e}{\det \mathbf{F}^e}, \quad (2.27)$$

The inequality (2.25) is re-written as

$$\sigma_{ij}^{NEQ} H_{jk}^e F_{im}^e H_{nk}^i \delta F_{mn}^i \geq 0, \quad (2.28)$$

Since the response of viscoelastic materials is usually rate-dependent, the variation expression is often replaced by the corresponding rate of change, e.g.,  $\delta \mathbf{F}^i$  is replaced by  $\delta \mathbf{F}^i / \delta t$  or  $\dot{\mathbf{F}}^i$ . Thus, inequality (2.28) is re-written as

$$\sigma_{ij}^{NEQ} L_{ij}^i \geq 0, \quad (2.29)$$

where  $\mathbf{L}^i$  is the inelastic part of the covariant velocity gradient, i.e.,

$$L_{ij} = L_{ij}^e + L_{ij}^i = \dot{F}_{im}^e H_{mj}^e + F_{im}^e \dot{F}_{mK}^i H_{Kp}^i H_{pj}^e. \quad (2.30)$$

Due to the symmetry of the true stress tensor, inequality (2.29) can be written in terms of the symmetric part of the inelastic velocity gradient, i.e., the inelastic stretch rate  $\mathbf{Q}^i = (\mathbf{L}^i + \mathbf{L}^{iT})/2$ , as

$$\sigma_{ij}^{NEQ} Q_{ij}^i \geq 0. \quad (2.31)$$

For inequality (2.31) to hold true, the non-equilibrium stress and the velocity gradient must satisfy a thermodynamic evolution equation in the form of (Boyce et al., 1989; Hong, 2011; Reese and Govindjee, 1998)

$$\mathcal{Q}_{mn}^i = \gamma_{mnij}^{-1} \sigma_{ij}^{NEQ}, \quad (2.32)$$

where  $\gamma^{-1}$  is a fourth rank mobility tensor which takes the form

$$\gamma^{-1} = \frac{1}{2\eta} \left( \mathbf{I}^4 - \frac{1}{3} \mathbf{I} \otimes \mathbf{I} \right). \quad (2.33)$$

with  $\mathbf{I}^4 = \frac{1}{2} (\delta_{ik} \delta_{jl} + \delta_{il} \delta_{jk})$  being the fourth order symmetric identity tensor,  $\mathbf{I}$  being the second order identity tensor, and  $\eta$  representing the shear viscosity.

## 2.3 Finite-deformation viscoelasticity of elastomers with nonlinear viscosity

From the above literature review, it can be seen that the viscosity  $\eta$  needs to be prescribed prior to the implementation of the developed modeling framework. In most of the existing works, the viscosity is assumed as a constant. However, the viscosity varies with the deformation of the material, which has also been proven by experiments (Pyckhout-Hintzen et al., 2013; Straube et al., 1995). To tackle this issue, de Gennes (1971) proposed one of the well-known models, i.e., the tube model, which was further developed by Doi and Edward (1998). According to the tube model (figure 2-3), a polymer chain C-D is assumed to be confined in a tube shape region with diameter  $a$  due to the constraint of the other polymer chains from surroundings. The axis of the tube C-D is defined as the primitive chain, and the polymer chain could be entangled (figure 2-3(a)) or crosslinked (figure 2-3(b)) with other chains in the ends. In the short time-scale, the motion of polymer chain can be considered as wriggling around the primitive chain within the tube. The effect of wriggle motion can be represented by several parameters like the diameter of tube and contour length of the primitive chain. In the long time-scale, the polymer chain moves along the tube, disengages from the original tube and shifts the ends. The deformation-dependent viscosity of material can be explained by the tube model. Particularly, when the elastomer is under large deformation, the diameter of tube significantly changes, which

affects the reptation ability of polymer chain. Following the concept of this tube model, a micro-mechanism inspired constitutive models for finite-deformation viscoelasticity of elastomers have been developed (Bergström and Boyce, 1998; Linder et al., 2011; Miehe et al., 2004). These models can capture the experimental data to some extent. Recently, based on the tube model and the theory of polymer dynamics (Doi and Edwards, 1988), a micro-macro constitutive model for finite-deformation viscoelasticity of elastomers is developed by Zhou et al (2018), in which the viscosity is deformation-dependent. This model is expected to be more accurate to capture the electromechanical response of dielectric elastomers, particularly when they undergo large deformation. Therefore, this modeling framework with the consideration of nonlinear viscosity motivates us to further investigate the viscous effect on the dynamic response and energy harvesting performance of DE-based devices such as oscillators and generators.

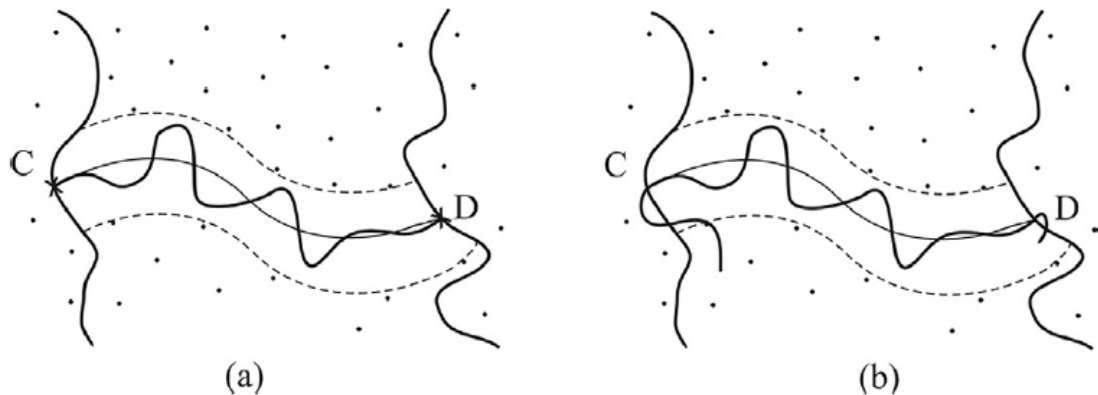


**Figure 2-3 Schematic of a polymer chain constrained in a tube region with primitive chain C-D (a) polymer chain end C and D crosslinked with other chains; (b) the polymer chain entangles with other polymer chains at C and D. (Zhou et al., 2018)**

## Chapter 3

### 3 Investigation on dynamic performance of viscoelastic dielectric elastomer oscillator considering material nonlinear viscosity

As a typical kind of soft electroactive materials, dielectric elastomers (DEs) are capable of producing large deformation under external stimuli, which makes them desirable materials for many practical applications in transduction technology, including tunable oscillators and resonators. The dynamic performance of such DE-based vibrational devices is strongly affected by material viscosity as well as electromechanical coupling. Moreover, as suggested by experiments and theoretical studies, DEs exhibit deformation-dependent relaxation process, which makes the modeling of the dynamic performance of DE-based devices more challenging. In this work, by adopting the state-of-art modeling framework of finite-deformation viscoelasticity, the effect of the nonlinear material viscosity on the in-plane oscillation and the frequency tuning of DE membrane oscillators is investigated. From the simulation results, it is found that the nonlinear viscosity only affects the transient state of the frequency tuning process. The modeling framework developed in this work is expected to provide useful guidelines for predicting the dynamic performance of DE-based vibrational devices as well as their optimal design.

#### 3.1 Introduction

As soft electroactive polymers, Dielectric elastomers (DEs) are capable of producing large deformation under electrical stimuli, which makes them desirable materials for electromechanical transducers (Pelrine et al., 2000). A common design of DE actuator consists of an elastomeric membrane sandwiched by two soft compliant electrodes on both sides. When a voltage is applied on the electrodes, the DE membrane contracts in thickness and expands in area (Pelrine et al., 2000). Due to their unique properties including large deformation capability, flexibility, and high energy density, DEs have been widely used to design functional actuators with different configurations in practical applications, such as soft robots, adaptive optical elements, programmable haptic surfaces, energy harvesters,

oscillators and resonators (Ahmadi et al., 2013; Anderson et al., 2010; Carpi et al., 2011; Kornbluh et al., 2002; O'Brien et al., 2010; O'Halloran et al., 2008; Pelrine et al., 2000).

The advantage of DE oscillators and resonators is that the oscillation of the membrane and the resonant frequency can be actively tuned by changing the applied alternating or static voltage (Li et al., 2012). This feature enables DE-based oscillators to be a promising alternative to traditional silicon-based devices. Early studies on analyzing the dynamic performance of DE-based oscillators and resonators mainly focused on their electromechanical response. For example, Feng et al. (2011) demonstrated the dynamic performance of a DE microbeam resonator under electromechanical load and investigated the oscillation of the device in terms of the quality factor (Q-factor) and the resonant frequency shift ratio. Li et al. (2012a) modeled the in-plane deformation and the frequency tuning of a plane membrane resonator using the Gent model (Gent, 1996). Kollosche et al. (2012) demonstrated how pre-stretching of DEs can change their voltage-induced deformation, electromechanical instability and loss-of-tension. However, DEs are proven to exhibit strong viscoelasticity in nature (Hong, 2011). The material viscoelasticity of DEs exerts a significant effect on their actuation response. Therefore, more efforts have been devoted to studying the viscoelastic effect on the behavior of DEs recently. For example, Yang et al. (2005) developed mechanics models accounting for the viscoelastic effect of DEs under uniaxial and biaxial loading conditions. Plante and Dubowsky (2007) studied the viscoelasticity of DEs with the Ogden model (Ogden, 1972) and experimentally demonstrated the effect of the stretching rate on the performance of DE actuators. Recently, based on the fully coupled field theory for DEs developed by Suo et al. (2008) and the finite-deformation viscoelasticity theory developed by Reese and Govindjee (1998), Hong (2011) has developed a constitutive model that can adopt most hyperelastic relations and evolution laws of viscoelastic solids to capture the viscoelastic response of DEs. Adopting the constitutive model by Hong (2011), Zhang et al. (2015) developed a dynamic model for homogeneously deformed viscoelastic DE actuator under equal-biaxial, uniaxial and pure shear forces. Based on the same framework, Zhou et al. (2014) demonstrated the effect of material viscoelasticity on the resonant frequency of DE resonators. Later, Zhou et al. (2016) further investigated the dynamic response of a DE membrane oscillator under a harmonic excitation. The above-mentioned studies assume the linearity of the material

viscosity when considering the viscoelastic deformation. In other words, the material viscosity is assumed as a constant in these studies. Nevertheless, according to the theory of polymer dynamics (Doi and Edwards, 1988), the viscosity of polymer chains in elastomers is deformation-dependent, i.e., nonlinear, especially when the elastomers undergo large deformation. This argument has also been confirmed by experiments (Hossain et al., 2012; Wang et al., 2016). In fact, much less effort has been devoted to addressing the effect of the nonlinear viscosity of DEs, which may also strongly influence the dynamic performance of DEs. Until recently, Zhou et al. (2018) incorporated the nonlinear material viscosity into the finite-deformation viscoelasticity theory by Reese and Govindjee (1998) to investigate the deformation of elastomers. In this work, the modeling framework by Zhou et al. (2018) will be further employed to study the frequency tuning process and the dynamic response of DE oscillators.

## 3.2 Models and formulations

In this work, the configuration of a commercial DE oscillator (Biggs and Hitchcock, 2010) is revisited which was developed by Artificial Muscle Inc. to investigate the dynamic performance of DE oscillators and resonators. As shown in figure 3-1, the DE oscillator consists of a DE membrane coated with two compliant electrodes on the top and bottom surfaces. Figure 3-1(a) shows the DE membrane in the undeformed state with dimensions  $L_1$ ,  $L_2$  and  $L_3$ . In figure 3-1(b), the DE is pre-stretched in area and attached to a rigid frame and a rigid bar of mass  $m$  with its two edges along 2-direction. The rigid bar is connected to the other side of the frame by a spring and a viscous damper. The stiffness of the spring and damping coefficient of the viscous damper are denoted as  $k$  and  $c$ , respectively. In the pre-stretched state, the elongation of the spring is denoted as  $\beta L_1$  and the dimensions of the DE membrane change to  $l_{1p}$ ,  $l_{2p}$  and  $l_{3p}$  with the pre-stretch ratios defined as  $\lambda_{1p} = l_{1p} / L_1$ ,  $\lambda_{2p} = l_{2p} / L_2$ , and  $\lambda_{3p} = l_{3p} / L_3$ . Then an electric voltage  $\Phi$  is applied to the compliant electrodes as shown in figure 3-1 (c). Under such an electrical load and forces from the spring and the viscous damper, the DE membrane further deforms to the current state with dimensions  $l_1$ ,  $l_2$ , and  $l_3$ . Consequently, the stretch ratios of the current state to



the undeformed state are defined as  $\lambda_1 = l_1 / L_1$ ,  $\lambda_2 = l_2 / L_2$ , and  $\lambda_3 = l_3 / L_3$ , respectively. In the current state, constrained by the rigid frame and the rigid bar, the DE membrane is under tensile forces  $P_1$  and  $P_2$  in 1 and 2 -directions. Moreover, the rigid bar is subjected to forces  $P_s$  from the spring and  $P_d$  from the viscous damper. The absolute position of the rigid bar in 1-direction is defined as  $x$ .

For such an oscillator configuration according to figure 3-1 (c), the motion equation of the rigid bar is expressed as,

$$\frac{P_s}{GL_2L_3} + \frac{P_p}{GL_2L_3} - \frac{P_1}{GL_2L_3} + \frac{m}{GL_2L_3} \frac{d^2x}{dt^2} = 0, \quad (3.1)$$

where the forces from the spring and the damper are  $P_s = (\beta - \lambda_1 + \lambda_{1p})L_1k$  and  $P_p = c \frac{dx}{dt}$ , respectively. It should be mentioned that, in addition to material fracture that could be prevented by limiting the stretches, there are other two possible failure modes of the DE, namely, loss-of-tension and electrical breakdown. To prevent loss-of-tension of the membrane, the in-plane forces in the DE membrane should be ensured as tensile forces, i.e.,  $P_1$  in 1-direction and  $P_2$  in 2-direction should be greater than 0. In addition, the applied voltage  $\Phi$  should be maintained below the electrical breakdown voltage of the DE. The breakdown voltage  $V_{EB}$  of the DE is determined by

$$\frac{V_{EB}}{L_3} \sqrt{\frac{\epsilon\epsilon_0}{G}} = d\lambda_1^{-1}\lambda_2^{-1}, \quad (3.2)$$

where  $d = E_{EB} \sqrt{\epsilon\epsilon_0 / G}$  and  $E_{EB}$  is the dielectric strength of the DE. (Koh et al., 2011b; Zhou et al., 2013)

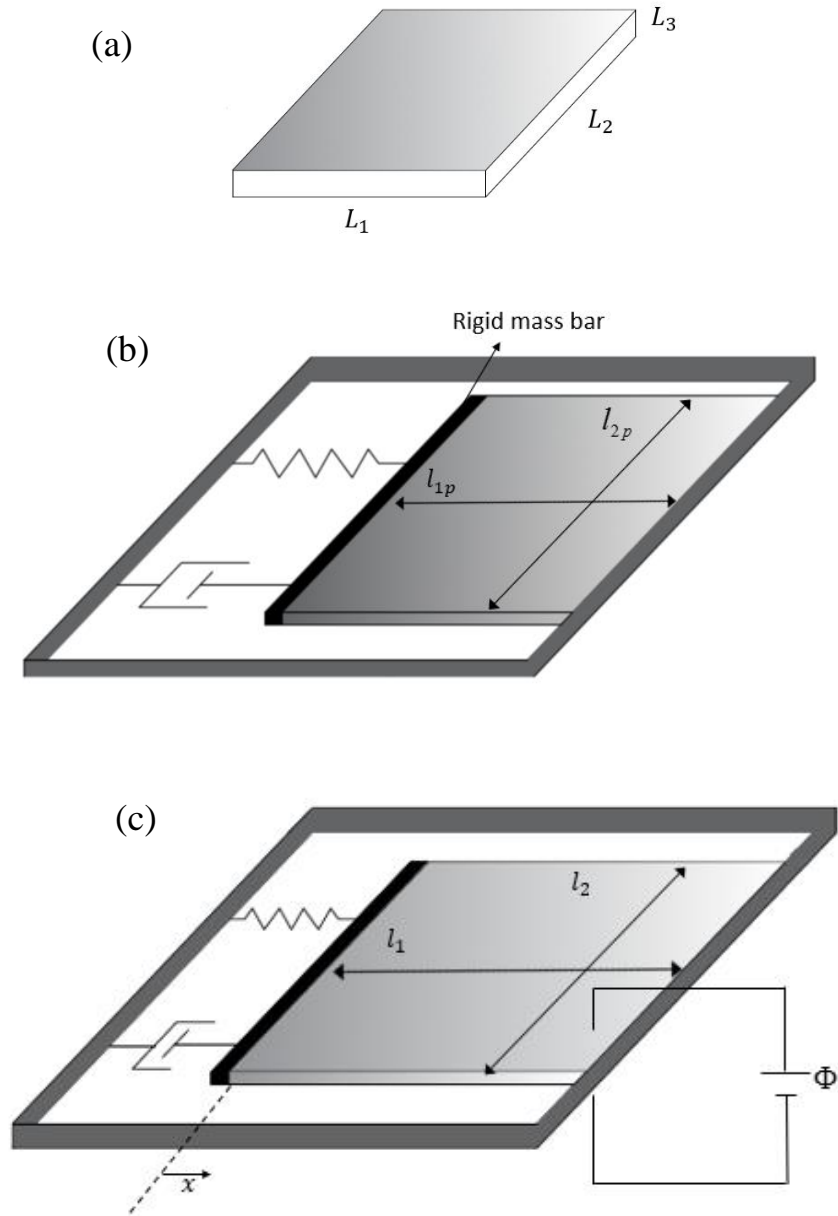


**Figure 3-1 Schematic of a DE membrane oscillator (a) undeformed state; (b) pre-stretched state; (c) current state**

Since DEs are known to exhibit viscoelastic properties, the deformation gradient  $\mathbf{F}$  of the DE membrane is commonly decomposed into an elastic component and an inelastic component in a multiplicative form (Hong, 2011), which gives

$$\mathbf{F} = \mathbf{F}^e \mathbf{F}^i, \quad (3.3)$$

$$\text{where } \mathbf{F} = \begin{pmatrix} \lambda_1 & 0 & 0 \\ 0 & \lambda_2 & 0 \\ 0 & 0 & \lambda_3 \end{pmatrix}, \mathbf{F}^i = \begin{pmatrix} \lambda_1^i & 0 & 0 \\ 0 & \lambda_2^i & 0 \\ 0 & 0 & \lambda_3^i \end{pmatrix}, \text{ and } \mathbf{F}^e = \begin{pmatrix} \lambda_1^e & 0 & 0 \\ 0 & \lambda_2^e & 0 \\ 0 & 0 & \lambda_3^e \end{pmatrix}.$$

under the current loading condition which assumes uniform deformation of the DE. The superscripts ‘e’ and ‘i’ represent the elastic and inelastic parts, respectively. Assuming material incompressibility of the DE (Hong, 2011; Li et al., 2012; Sheng et al., 2014; Yong et al., 2011; Zhou et al., 2014), the stretch ratio satisfies  $\lambda_3 = 1/\lambda_1\lambda_2$ ,  $\lambda_3^e = 1/\lambda_1^e\lambda_2^e$  and  $\lambda_3^i = 1/\lambda_1^i\lambda_2^i$ . Furthermore, the total Helmholtz free energy  $w$  of the deformed DE membrane consists of two parts. One is the equilibrium Helmholtz free energy density  $W^{EQ}$ , which is associated with both the total deformation and the applied electric voltage  $\Phi$ . The other part is the non-equilibrium Helmholtz free energy density  $W^{NEQ}$ , which is only related to the elastic deformation. Therefore,  $W = W^{EQ}(\lambda_1, \lambda_2, V) + W^{NEQ}(\lambda_1^e, \lambda_2^e)$ . It is worth noticing that the electric field is assumed to be in equilibrium as the electric field always reaches the equilibrium state much faster than the mechanical deformation (Hong, 2011). According to the work of Huang and Suo (2012) the equilibrium Helmholtz free energy density  $W^{EQ}$  takes the form of,

$$W^{EQ} = W_s(\lambda_1, \lambda_2) + \frac{\varepsilon\varepsilon_0}{2} \left(\frac{\Phi}{L_3}\right)^2 \lambda_1^2 \lambda_2^2, \quad (3.4)$$

where  $W_s(\lambda_1, \lambda_2)$  is the strain energy density function of the elastomer, and the second term is the free energy associated with the polarization,  $\varepsilon_0$  is the dielectric permittivity of the vacuum and  $\varepsilon$  is the relative dielectric constant of the DE. Here, the Gent model is adopted (Gent, 1996) as the strain energy density function for both the equilibrium and non-equilibrium Helmholtz free energy density, i.e.,

$$W_s = -\frac{G^{EQ} J_{\text{lim}}^{EQ}}{2} \ln \left( 1 - \frac{\lambda_1^2 + \lambda_2^2 + \lambda_1^{-2} \lambda_2^{-2} - 3}{J_{\text{lim}}} \right) \quad (3.5)$$

$$W^{NEQ} = -\frac{G^{NEQ} J_{\text{lim}}^{NEQ}}{2} \ln \left( 1 - \frac{(\lambda_1^e)^2 + (\lambda_2^e)^2 + (\lambda_1^e \lambda_2^e)^{-2} - 3}{J_{\text{lim}}} \right), \quad (3.6)$$

where  $G^{EQ}$  and  $G^{NEQ}$  are the equilibrium shear modulus and non-equilibrium shear modulus,  $J_{\text{lim}}^{EQ}$  is a dimensionless parameter related to the limiting stretch of the DE, while  $J_{\text{lim}}^{NEQ}$  is determined by the stretching limit of the elastic component of the DE.

When the DE in the current state is perturbed, the change of the total Helmholtz free energy equals to the work done by the tensile force  $P_1$  and  $P_2$ , the inertia force and the voltage  $\Phi$ , resulting in

$$L_1 L_2 L_3 \left( \frac{\partial W}{\partial \lambda_1} \delta \lambda_1 + \frac{\partial W}{\partial \lambda_2} \delta \lambda_2 \right) = P_1 L_1 \delta \lambda_1 + P_2 L_2 \delta \lambda_2 + \Phi \delta Q - L_2 L_3 \frac{L_1^3}{3} \rho \frac{d^2 \lambda_1}{dt^2} \delta \lambda_1, \quad (3.7)$$

where  $\rho$  is the mass density of the DE and the charge on the DE is expressed as  $Q = \Phi \varepsilon \varepsilon_0 \lambda_1^2 \lambda_2^2 L_1 L_2 / L_3$ . It can be noticed that the work done by the inertia force in the thickness direction is ignored in equation (3.7) since the oscillator only vibrates in 1-direction and  $L_3 \ll L_1$ .

Considering that  $\delta \lambda_1$  and  $\delta \lambda_2$  are any arbitrary small variations, substituting equations (3.4) -(3.6) into (3.7) leads to:

$$\begin{aligned} \frac{P_1}{GL_2 L_3} &= \frac{\chi J_{\text{lim}} (\lambda_1 - \lambda_1^{-3} \lambda_2^{-2})}{J_{\text{lim}} - \lambda_1^2 - \lambda_2^2 - \lambda_1^{-2} \lambda_2^{-2} + 3} \\ &+ \frac{(1-\chi) J_{\text{lim}} (\lambda_1 (\lambda_1^i)^{-2} - \lambda_1^{-3} \lambda_2^{-2} (\lambda_1^i)^2 (\lambda_2^i)^{-2})}{J_{\text{lim}} - \left(\frac{\lambda_1}{\lambda_1^i}\right)^2 - \left(\frac{\lambda_2}{\lambda_2^i}\right)^2 - \left(\frac{\lambda_1 \lambda_2}{\lambda_1^i \lambda_2^i}\right)^{-2} + 3} + \frac{L_1^2 \rho}{3G} \frac{d^2 \lambda_1}{dt^2} - \frac{\varepsilon \varepsilon_0}{G} \left(\frac{\Phi}{L_3}\right)^2 \lambda_1 \lambda_2^2 \end{aligned} \quad (3.8)$$

$$\begin{aligned} \frac{P_2}{GL_1 L_3} &= \frac{\chi J_{\text{lim}} (\lambda_2 - \lambda_2^{-3} \lambda_1^{-2})}{J_{\text{lim}} - \lambda_1^2 - \lambda_2^2 - \lambda_1^{-2} \lambda_2^{-2} + 3} \\ &+ \frac{(1-\chi) J_{\text{lim}} (\lambda_2 (\lambda_2^i)^{-2} - \lambda_2^{-3} \lambda_1^{-2} (\lambda_1^i)^2 (\lambda_2^i)^{-2})}{J_{\text{lim}} - \left(\frac{\lambda_1}{\lambda_1^i}\right)^2 - \left(\frac{\lambda_2}{\lambda_2^i}\right)^2 - \left(\frac{\lambda_1 \lambda_2}{\lambda_1^i \lambda_2^i}\right)^{-2} + 3} - \frac{\varepsilon \varepsilon_0}{G} \left(\frac{\Phi}{L_3}\right)^2 \lambda_2 \lambda_1^2, \end{aligned} \quad (3.9)$$

where  $G = G^{EQ} + G^{NEQ}$  and  $\chi = G^{EQ} / G$  ( $0 \leq \chi \leq 1$ ).  $\chi$  represents the fraction of the time-independent polymer networks in the elastomer, which equals to 1 for a purely elastic medium, while 0 for a viscous fluid.

Furthermore, the inelastic stretch ratio ( $\lambda_1^i$  and  $\lambda_2^i$ ) in equations (3.8) and (3.9) must satisfy the thermodynamic evolution law (Reese and Govindjee, 1998), i.e.,

$$-\frac{1}{2} \mathbf{F} \frac{d \left[ (\mathbf{C}^i)^{-1} \right]}{dt} \mathbf{F}^T (\mathbf{b}^e)^{-1} = \boldsymbol{\gamma}^{-1} : \boldsymbol{\tau}_{NEQ}, \quad (3.10)$$

where  $\mathbf{C}^i = (\mathbf{F}^i)^T \mathbf{F}^i$ ,  $(\mathbf{b}^e)^{-1} = (\mathbf{F}^e)^T \mathbf{F}^e$ ,  $\boldsymbol{\tau}_{NEQ} = 2 \mathbf{F}^e \frac{\partial W^{NEQ}}{\partial \mathbf{C}^e} (\mathbf{F}^e)^T$ ,  $\mathbf{C}^e = (\mathbf{F}^e)^T \mathbf{F}^e$  and  $\boldsymbol{\gamma}^{-1}$  is an isotropic rank four tensor. According to the work of (Reese and Govindjee, 1998)  $\boldsymbol{\gamma}^{-1}$  takes the form

$$\boldsymbol{\gamma}^{-1} = \frac{1}{2\eta} \left( \mathbf{I}^4 - \frac{1}{3} \mathbf{I} \otimes \mathbf{I} \right), \quad (3.11)$$

where  $\mathbf{I}^4 = \frac{1}{2} (\delta_{ik} \delta_{jl} + \delta_{il} \delta_{jk})$  is an isotropic rank-four mobility tensor,  $\mathbf{I}$  is the second order identity tensor, and  $\eta$  represents the shear viscosity. According to this thermodynamic evolution law, the time-dependent inelastic stretch ratios are expressed as

$$\begin{aligned} \frac{d\lambda_1^i}{dt} &= \frac{G^{NEQ} J_{\text{lim}} \lambda_1^i}{6\eta \left[ J_{\text{lim}} - \left( \frac{\lambda_1}{\lambda_1^i} \right)^2 - \left( \frac{\lambda_2}{\lambda_2^i} \right)^2 - \left( \frac{\lambda_1}{\lambda_1^i} \right)^{-2} \left( \frac{\lambda_2}{\lambda_2^i} \right)^{-2} + 3 \right]} \\ &\quad \times \left[ 2 \left( \frac{\lambda_1}{\lambda_1^i} \right)^2 - \left( \frac{\lambda_2}{\lambda_2^i} \right)^2 - \left( \frac{\lambda_1^{-1} \lambda_2^{-1}}{(\lambda_1^i)^{-1} (\lambda_2^i)^{-1}} \right)^2 \right] \end{aligned} \quad (3.12)$$

$$\begin{aligned} \frac{d\lambda_2^i}{dt} &= \frac{G^{NEQ} J_{\text{lim}} \lambda_2^i}{6\eta \left[ J_{\text{lim}} - \left( \frac{\lambda_1}{\lambda_1^i} \right)^2 - \left( \frac{\lambda_2}{\lambda_2^i} \right)^2 - \left( \frac{\lambda_1}{\lambda_1^i} \right)^{-2} \left( \frac{\lambda_2}{\lambda_2^i} \right)^{-2} + 3 \right]} \\ &\quad \times \left[ 2 \left( \frac{\lambda_2}{\lambda_2^i} \right)^2 - \left( \frac{\lambda_1}{\lambda_1^i} \right)^2 - \left( \frac{\lambda_1^{-1} \lambda_2^{-1}}{(\lambda_1^i)^{-1} (\lambda_2^i)^{-1}} \right)^2 \right] \end{aligned} \quad (3.13)$$

It should be noted that  $\eta$  is the viscosity of the material in the current state, which depends on the deformation of the DE and should be constitutively prescribed to obtain the inelastic stretch ratios as shown in equations (3.12) and (3.13). Here, the theory of polymer dynamics by Doi and Edwards (1988) will be used to determine the nonlinear viscosity  $\eta$ .

According to their theory, the viscosity  $\eta$  of elastomers originates from the diffusion of the polymer chains in the material and a polymer chain (A-B) is considered to confine in a tube-like region due to topological constraints (see figure 3.2 (a)). Moreover, the diffusion process of a polymer chain can be classified based on time-scale. In the short time-scale the polymer chain wriggles within the tube, while in the long time-scale, the polymer chain reptates along the tube. Therefore, the viscosity  $\eta$  can be expressed in terms of the tube diameter  $a$  as,

$$\eta = \frac{1}{12} \frac{\zeta N^3 b_0^4 G_0}{k_B T \langle a \rangle^2}, \quad (3.14)$$

where  $\zeta$  is the monomer friction constant,  $N$  is the polymerization degree of chains,  $b_0$  is the effective bond length between monomers,  $G_0$  is the shear relaxation modulus in the undeformed state,  $T$  is the temperature,  $k_B$  is the Boltzmann constant and  $\langle * \rangle$  is the expectation operator of a parameter. Also, the axis of the tube confining chain A-B is defined as the primitive chain of the polymer chain. According to the work of Doi and Edwards (1988), the tube diameter  $a$  is a function of the primitive length  $L$  of the polymer chain and the end-to-end vector  $\mathbf{R}$  of the primitive chain, i.e.,  $\langle a \rangle = \langle \mathbf{R}^2 \rangle / \langle L \rangle$  (see figure 3-2). When the deformation of the material is small,  $\mathbf{R}$  and  $L$  can be assumed as unchanged, which leads to a constant tube diameter  $a$  and thus a constant viscosity  $\eta$ . However, when the material undergoes large deformation, both  $L$  and  $\mathbf{R}$  should change with the macroscopic deformation (Doi and Edwards, 1988; Zhou et al., 2018), i.e.,

$\langle L \rangle = \int \frac{|\mathbf{F} \cdot \mathbf{u}|}{4\pi} L d^2 \mathbf{u}$  and  $\langle \mathbf{R}^2 \rangle = \int |\mathbf{F} \cdot \mathbf{R}|^2 f_0(\mathbf{R}) d^3 R$ , where  $\mathbf{u}$  is the unit tangent vector at a contour position of the polymer chain in the reference state,  $f_0(\mathbf{R})$  is the statistical distribution function of the end-to-end vector  $\mathbf{R}$  in the reference state and  $\mathbf{F}$  is the

deformation gradient. Therefore, the nonlinear viscosity of the elastomer can be determined as,

$$\frac{\eta}{\eta_0} = \frac{a_0^2}{\langle a \rangle^2} = \left\{ \frac{\langle \mathbf{R}^2 \rangle_0 \frac{|\mathbf{F} \cdot \mathbf{u}|}{4\pi} d^2 \mathbf{u}}{\int |\mathbf{F} \cdot \mathbf{R}|^2 f_0(\mathbf{R}) d^3 R} \right\}^2, \quad (3.15)$$

where  $a_0$  is the tube diameter and  $\eta_0 = \frac{1}{12} \frac{\zeta N^3 b_0^4 G_0}{k_b T a_0^2}$  is the viscosity in the reference state.

For the convenience of expression, the viscosity ratio in equation (3.15) can be expressed as,

$$\frac{\eta}{\eta_0} = \frac{1}{\alpha(\mathbf{F})^2}, \quad (3.16)$$

$$\text{with } \frac{1}{\alpha(\mathbf{F})} = \frac{\langle \mathbf{R}^2 \rangle_0 \frac{|\mathbf{F} \cdot \mathbf{u}|}{4\pi} d^2 \mathbf{u}}{\int |\mathbf{F} \cdot \mathbf{R}|^2 f_0(\mathbf{R}) d^3 R}.$$

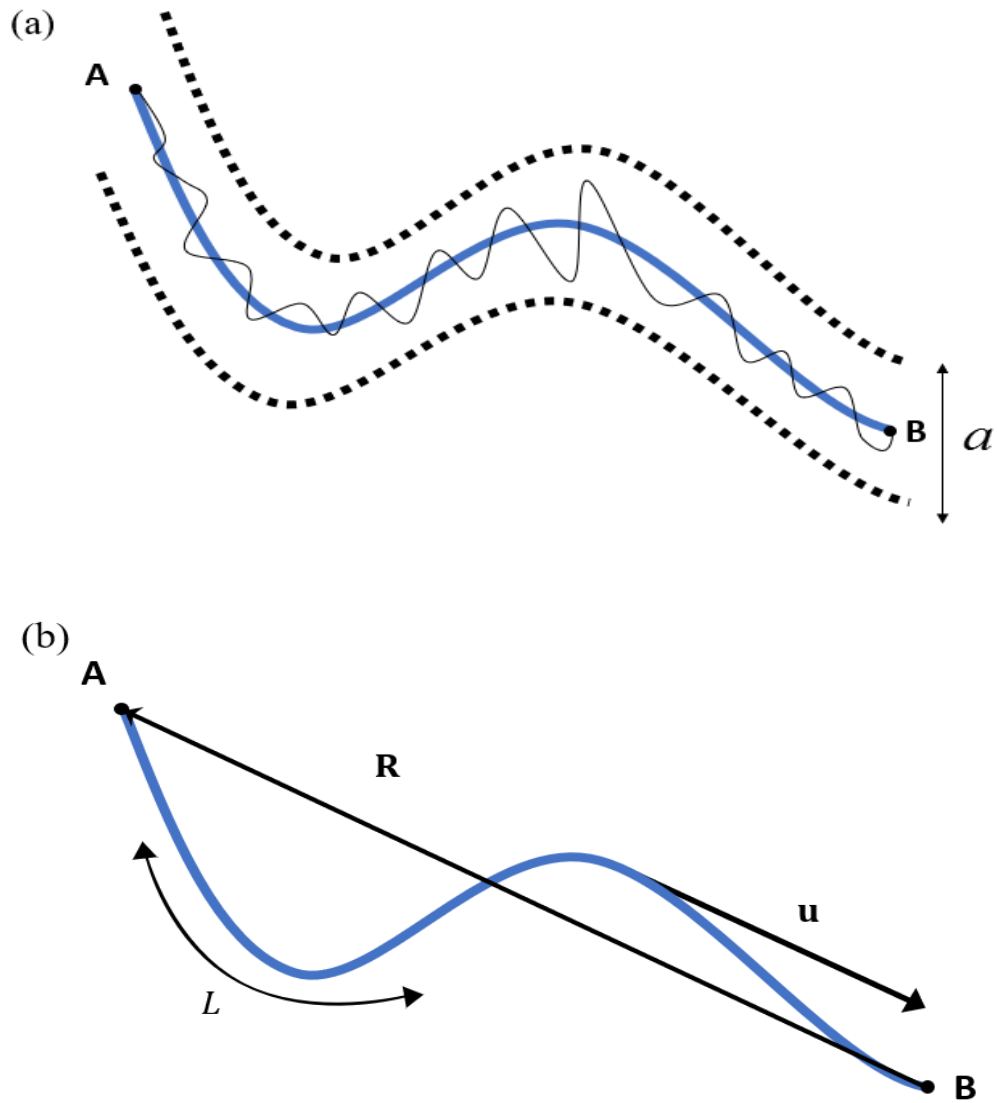


**Figure 3-2 Illustration of a polymer chain confined in a tube-like region with the tube diameter of  $a$ . (a) Polymer chain A-B is represented by its primitive chain (blue color); (b) dimensions of the primitive chain.**

### 3.3 Resonant frequency of an oscillator

For the oscillator shown in figure 1, the deformation of the DE is fixed in 2-direction, i.e.,  $\lambda_2 = \lambda_{2p}$ , and  $x = (\lambda_{1p} - \lambda_1)L_1$ , then equation (3.1) can be reduced to a second order differential equation as,



$$\frac{d^2 \lambda_1}{dt^2} + a_1 \frac{d \lambda_1}{dt} + g(\lambda_1, \lambda_1^i, \lambda_2^i, V^*) = 0 \quad (3.17)$$

where

$$g = a_2 \left\{ \begin{array}{l} \frac{\chi J_{\text{lim}}^{\text{EQ}} (\lambda_1 - \lambda_1^{-3} \lambda_2^{-2})}{J_{\text{lim}}^{\text{EQ}} - \lambda_1^2 - \lambda_2^2 - \lambda_1^{-2} \lambda_2^{-2} + 3} \\ (1 - \chi) J_{\text{lim}}^{\text{NEQ}} \left[ \lambda_1 (\lambda_1^i)^{-2} - \lambda_1^{-3} \lambda_2^{-2} (\lambda_1^i)^2 (\lambda_2^i)^2 \right] \\ J_{\text{lim}}^{\text{NEQ}} - \left( \frac{\lambda_1}{\lambda_1^i} \right)^2 - \left( \frac{\lambda_2}{\lambda_2^i} \right)^2 - \left( \frac{\lambda_1 \lambda_2}{\lambda_1^i \lambda_2^i} \right)^{-2} + 3 \\ - (V^*)^2 \lambda_1 \lambda_2^2 - \frac{(\beta - \lambda_1 + \lambda_{1p}) L_1 k}{GL_2 L_3} \end{array} \right\}$$

Here, the dimensionless voltage is defined as  $V^* = \Phi \sqrt{\epsilon \epsilon_0 / G} / L_3$ ,

$a_1 = \frac{cL_1}{GL_2 L_3} / \left( \frac{mL_1}{GL_2 L_3} + \frac{L_1^2}{3G} \rho \right)$  and  $a_2 = 1 / \left( \frac{mL_1}{GL_2 L_3} + \frac{L_1^2}{3G} \rho \right)$ . To study the resonant frequency of

the oscillator, it adopts the commonly used perturbation method in the literature (Li et al., 2012; Zhou et al., 2014; Zhu et al., 2010). When the membrane is subjected to a small perturbation of amplitude  $\Delta(t)$  in 1-direction at time  $t$ , the total stretch ratio of the membrane in that direction can be expressed as

$$\lambda_1 = \lambda_1' + \Delta(t) \quad (3.18)$$

where  $\lambda_1'$  is the stretch ratio of the DE in the kinetic equilibrium state in 1-direction before the perturbation. Meanwhile, by combining equations (3.17) and (3.18), and expanding the equation into Taylor series, equation (3.17) becomes

$$\frac{d^2 \Delta}{dt^2} + a_1 \frac{d \Delta}{dt} + \frac{\partial g(\lambda_1', \lambda_1^i, \lambda_2^i, V^*)}{\partial \lambda_1} \Delta = 0 \quad (3.19)$$

Therefore, the resonant frequency can be determined as

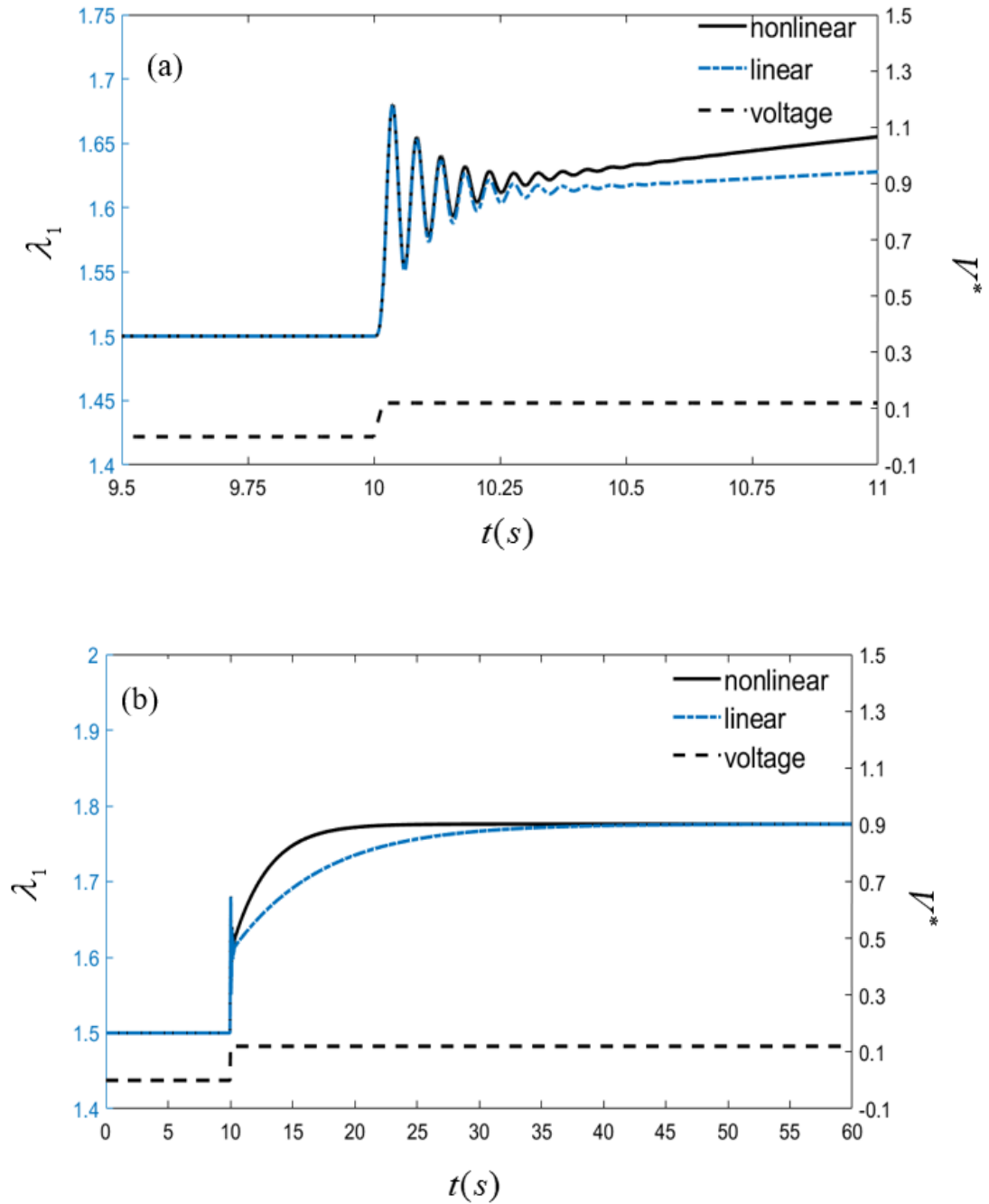
$$\begin{aligned}
\omega_n^2 &= \frac{\partial g(\lambda_1^i, \lambda_1^i, \lambda_2^i, V^*)}{\partial \lambda_1} \\
&= a_2 \left\{ \frac{\chi J_{\text{lim}}^{\text{EQ}} (1 + 3\lambda_1^{-4} \lambda_2^{-2})}{J_{\text{lim}}^{\text{EQ}} - \lambda_1^2 - \lambda_2^2 - \lambda_1^{-2} \lambda_2^{-2} + 3} + \frac{2\chi J_{\text{lim}}^{\text{EQ}} (\lambda_1 - \lambda_1^{-3} \lambda_2^{-2})^2}{(J_{\text{lim}}^{\text{EQ}} - \lambda_1^2 - \lambda_2^2 - \lambda_1^{-2} \lambda_2^{-2} + 3)^2} - (V^*)^2 \lambda_2^2 + \frac{kL_1}{GL_2L_3} \right. \\
&\quad \left. + \frac{(1-\chi) J_{\text{lim}}^{\text{NEQ}} \left[ (\lambda_1^i)^{-2} + 3\lambda_1^{-4} \lambda_2^{-2} (\lambda_1^i)^2 (\lambda_2^i)^2 \right]}{J_{\text{lim}}^{\text{NEQ}} - \left( \frac{\lambda_1}{\lambda_1^i} \right)^2 - \left( \frac{\lambda_2}{\lambda_2^i} \right)^2 - \left( \frac{\lambda_1 \lambda_2}{\lambda_1^i \lambda_2^i} \right)^{-2} + 3} + \frac{2(1-\chi) J_{\text{lim}}^{\text{NEQ}} \left[ \lambda_1 (\lambda_1^i)^{-2} - \lambda_1^{-3} \lambda_2^{-2} (\lambda_1^i)^2 (\lambda_2^i)^2 \right]^2}{\left[ J_{\text{lim}}^{\text{NEQ}} - \left( \frac{\lambda_1}{\lambda_1^i} \right)^2 - \left( \frac{\lambda_2}{\lambda_2^i} \right)^2 - \left( \frac{\lambda_1 \lambda_2}{\lambda_1^i \lambda_2^i} \right)^{-2} + 3 \right]^2} \right\} \quad (3.20)
\end{aligned}$$

As it can be seen from the expression of the resonant frequency in equation (3.20), it is a function of the time-dependent inelastic stretch ratios  $\lambda_1^i$  and  $\lambda_2^i$ . Therefore,  $\omega_n$  is an instant resonant frequency of the oscillator at time  $t$ .

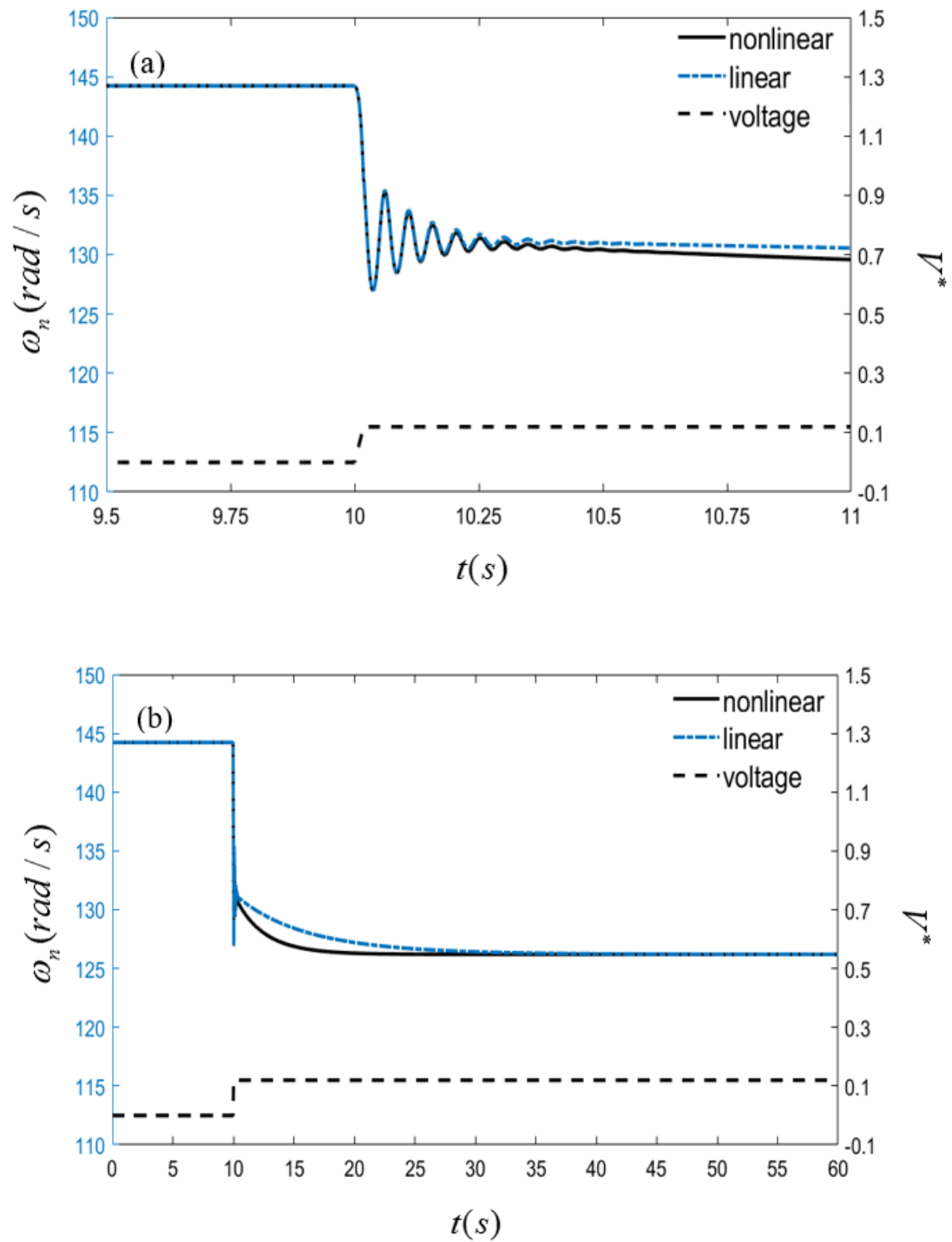
As demonstrated in the literature, the resonant frequency of a DE oscillator can be actively tuned by applying a voltage to the DE membrane (Li et al., 2012; Zhou et al., 2016). Here, the frequency tuning process of DE oscillators with the new material model accounting for the nonlinear viscosity is revisited. Figures 3-3 (a) and 3-3 (b) show the change of the stretch ratio during a typical frequency tuning process. Also, figure 3-4 (a) and figure 3-4 (b) plot the variation of the resonant frequency  $\omega_n$  during the same process. The results from both the linear and nonlinear viscosity models are also compared in these figures. The geometric and material parameters take the values from the previous studies (Chiang Foo et al., 2012a; Zhou et al., 2016), i.e.,  $\alpha = 4, \beta = 1, a_1 = 20, a_2 = 10^4, d = 5,$

$J_{\text{lim}}^{\text{EQ}} = 110, J_{\text{lim}}^{\text{NEQ}} = 55, \chi = 0.3,$  and the relaxation time  $\tau_0 = \frac{\eta_0}{G^{\text{NEQ}}} = 3$  in the reference state. Moreover, in the simulation, it is ensured that the applied voltage is lower than the electrical breakdown voltage of the DE membrane, and the loss-of-tension of the membrane is also avoided. At the very beginning, the oscillator in the pre-stretched state (with  $\lambda_{1p} = 1.5$  and  $\lambda_{2p} = 3$ ) is fully relaxed. Therefore, both the stretch ratio  $\lambda_1$  and the resonant frequency  $\omega_n$  remain unchanged. After sufficient time, for example at  $t = 10$  s, a voltage is applied to the DE membrane at a rate of  $dV^*/dt = 6.667$  and the voltage is then fixed as  $V^* = 0.125$  afterwards. The response curves for both the linear and nonlinear viscosity models demonstrate the same trend. It is observed that the applied voltage causes

a fast rise of the stretch ratio  $\lambda_1$  and a sudden drop of the resonant frequency  $\omega_n$ . After the voltage is applied, both the stretch ratio and the resonant frequency fluctuate with a decaying amplitude, which is a typical transient response for a spring-damper system. During this fluctuation, energy of the system dissipates mainly through the damper. After such a period, the stretch ratio starts to increase, while the resonant frequency starts to gradually decrease. This is mainly due to the stress relaxation of the DE membrane. From figure 3-3 (b) and figure 3-4 (b), it is observed that after sufficient time, the stretch ratio and the resonant frequency eventually become steady, which indicates that the DE membrane is fully relaxed again and has reached an equilibrium state and the resonant frequency remains as a constant thereafter. The value of the resonant frequency at this steady state is defined as the tuned frequency by the applied voltage. It is observed that the difference of the response curves between the nonlinear viscosity model and the linear viscosity model is considerable during the transient state, while the DE membrane reaches the same steady state for both the linear and nonlinear models. Moreover, the DE membrane reaches the steady state faster when the nonlinear viscosity is considered. The reason behind this phenomenon is that, as the stretch ratio increases with the applied voltage from the reference state to the current state,  $\alpha(\mathbf{F})$  rises rapidly. Therefore, the viscosity  $\eta$  decreases rapidly since it is inversely proportional to the second order of  $\alpha(F)$  as shown by equation (3.16). In other words, the nonlinear viscosity  $\eta$  decreases from the reference state to current state. Thus, the DE membrane relaxes faster when the nonlinear material viscosity is considered.

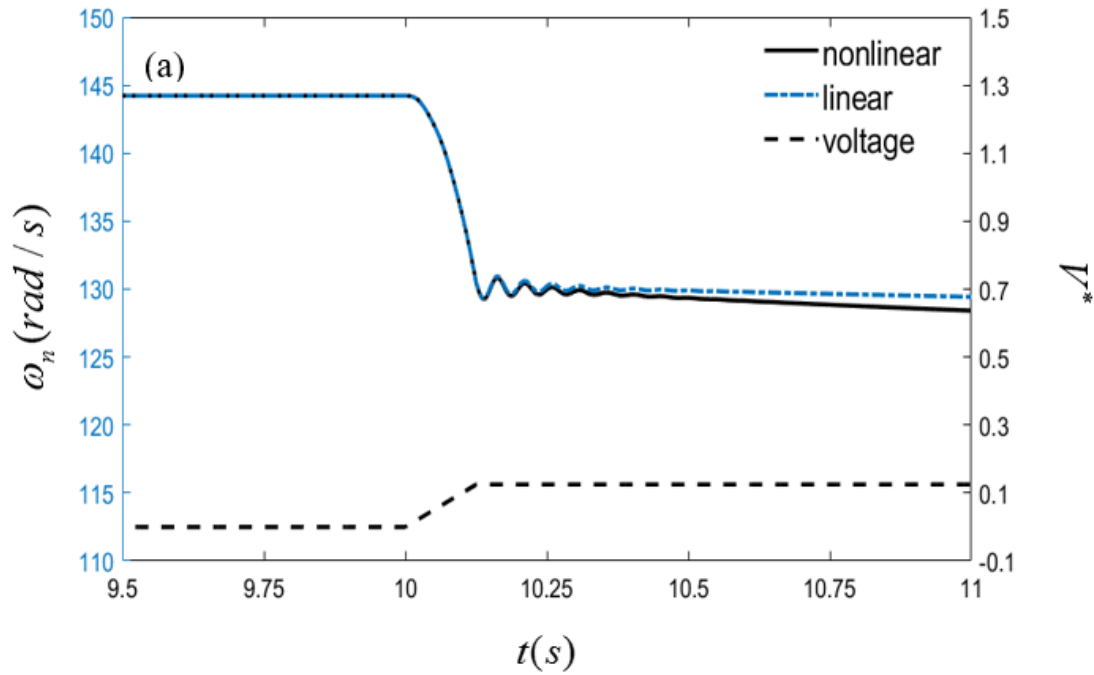


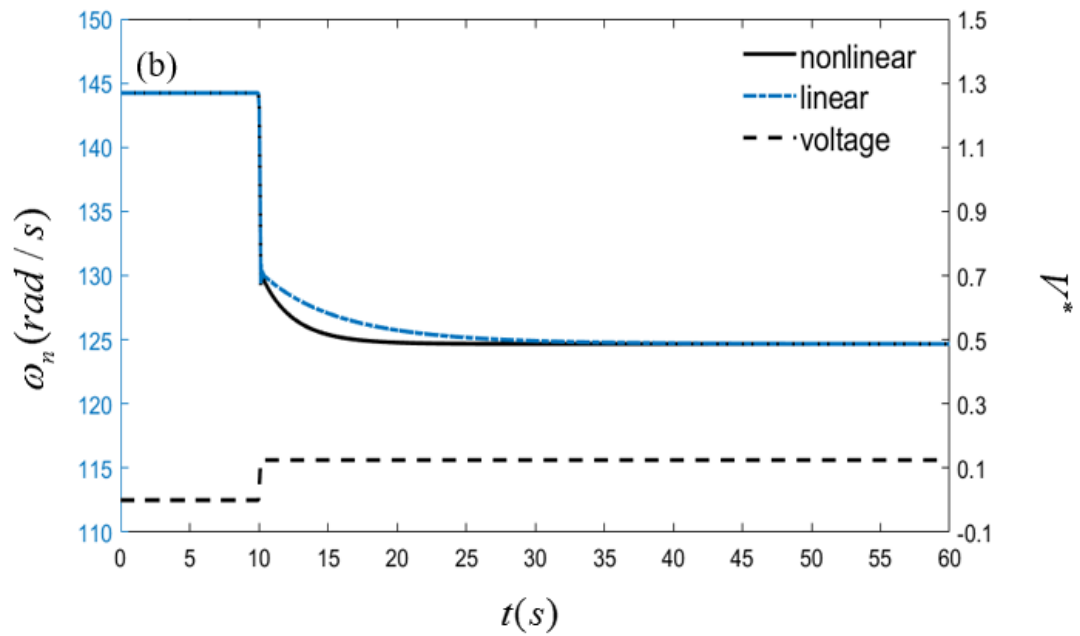
**Figure 3-3** Variation of stretch ratio with time for two different viscosity models when a static voltage is applied. (a) Time interval is from 9.5 s to 11 s; (b) time interval is from 0 s to 60 s.



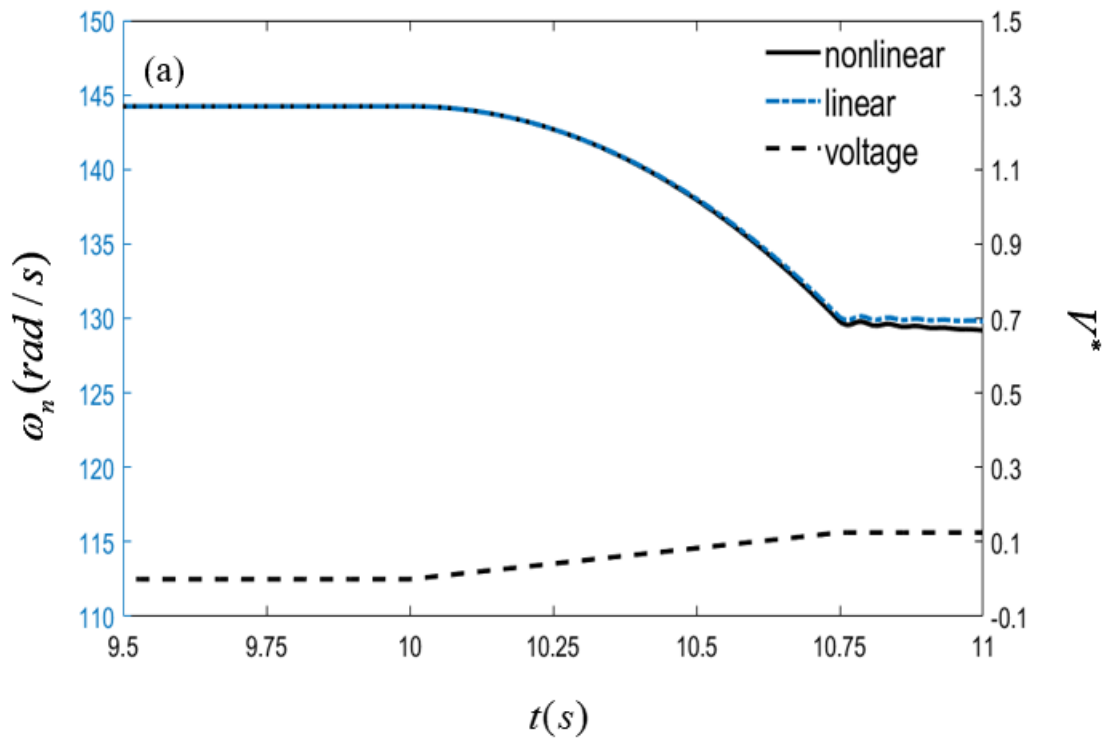
**Figure 3-4** Frequency tuning process for two different viscosity models when a static voltage is applied. (a) Time interval is from 9.5 s to 11 s; (b) time interval is from 0 s to 60 s.

The effect of the applied voltage rate on the tuned frequency of the DE oscillator is demonstrated in figures 3-5 and 3-6 with loading rate  $dV^* / dt = 1$  and  $dV^* / dt = 0.1667$ , respectively. At a higher rate of the applied voltage, there is more fluctuation on the resonant frequency, which means that the damper has more dominant effect. However, the loading rate has no effect on the tuned frequency, which is only a function of the value of the applied voltage. Furthermore, figure 3-7 illustrates a comparison of the tuned frequency between a viscoelastic ( $\chi = 0.5$ ) DE resonator and a purely elastic DE resonator. It can be noticed that the viscoelastic DE membrane resonator has a tuned frequency range about 50% narrower than the purely elastic one. It should be mentioned that nonlinear material viscosity does not change the tuned frequency of the oscillator.





**Figure 3-5 Effect of loading rate of the applied voltage ( $dV^*/dt = 1$ ) on frequency tuning for two different viscosity models. (a) Time interval is from 9.5 s to 11 s; (b) time interval is from 0 s to 60 s.**



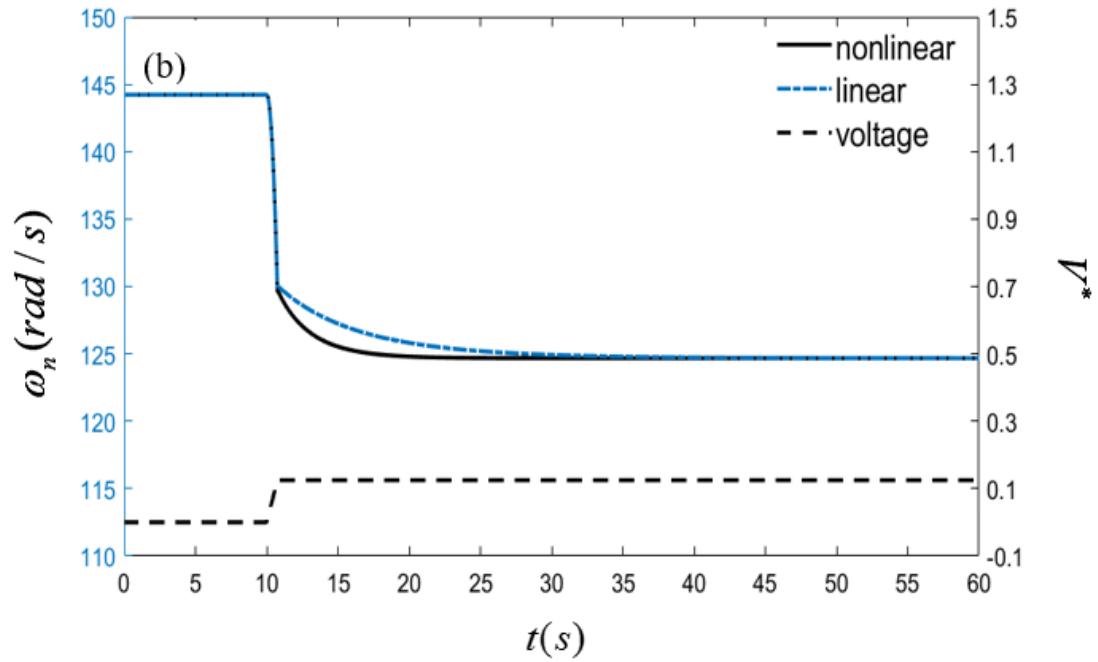


**Figure 3-6 Effect of loading rate of the applied voltage ( $dV^*/dt=0.1667$ ) on frequency tuning for two different viscosity models. (a) Time interval is from 9.5 s to 11 s; (b) time interval is from 0 s to 60 s.**



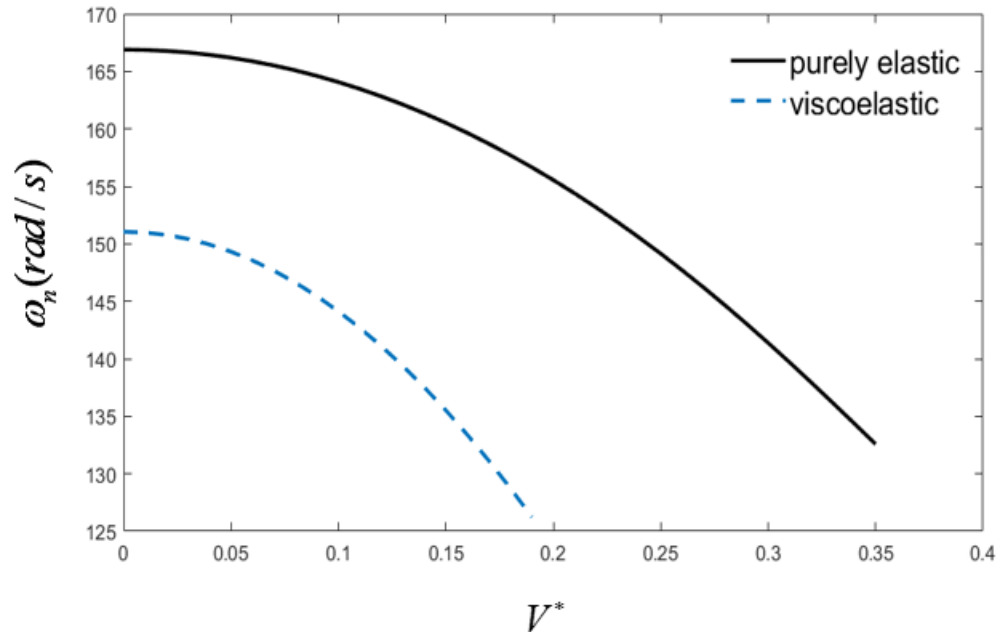


**Figure 3-7 Variation of the tuned frequency for purely elastic and viscoelastic DE resonators within a certain range of applied voltage.**

To further investigate the influence of the nonlinear material viscosity on the dynamic response of DE-based oscillators, an AC voltage  $V^* = p \sin(q\omega_n t)$  is applied to the DE membrane to generate oscillation.  $p$  and  $q$  are parameters that govern the amplitude and frequency of the alternating voltage. As shown in figure 3-8, the difference between the linear viscosity and nonlinear viscosity models is mainly reflected during the transient response of the DE oscillator.

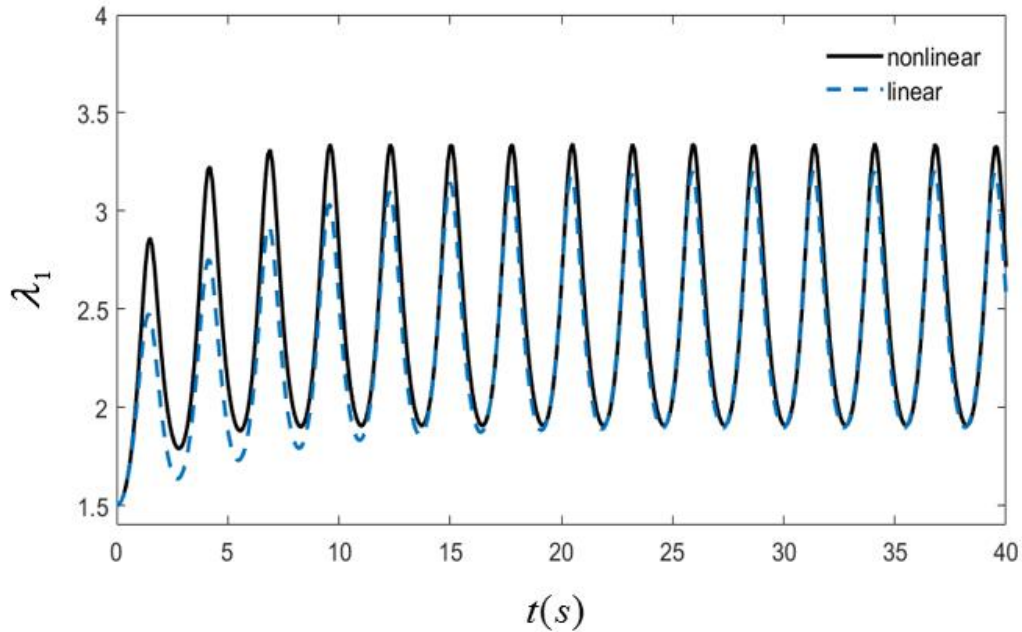
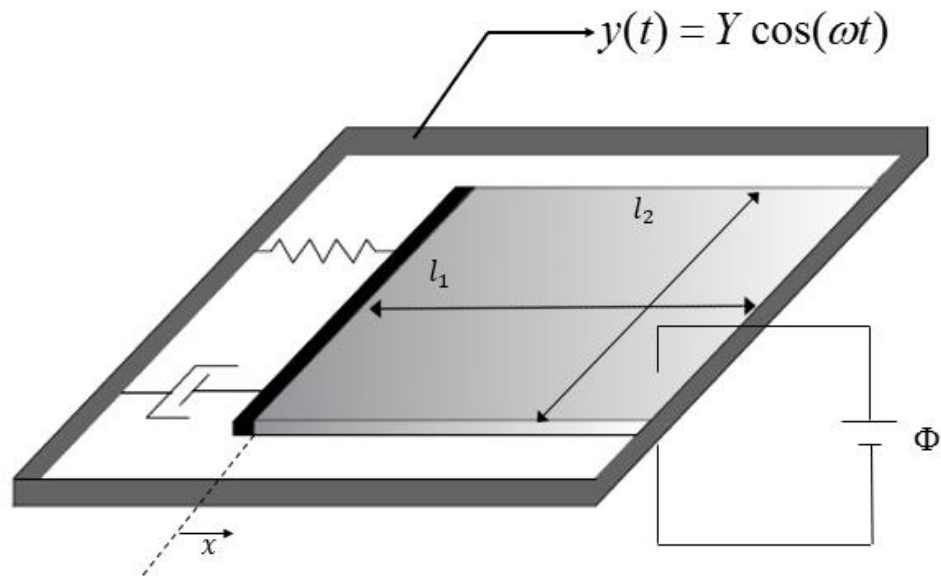


**Figure 3-8 Variation of the stretch ratio with time (0s to 60s) for two different viscosity models when an AC voltage is applied.**

### 3.4 Forced response of an oscillator

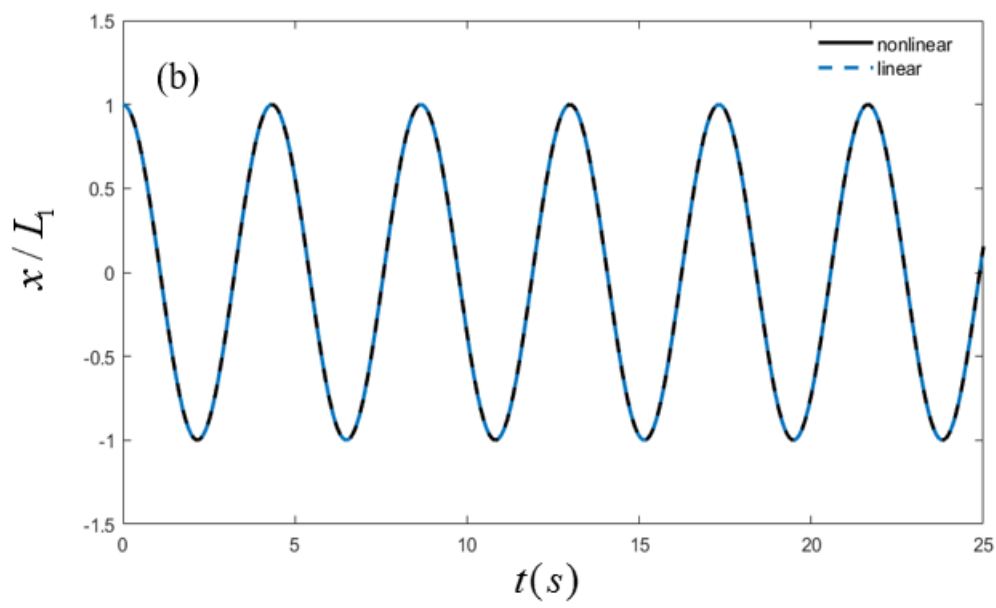
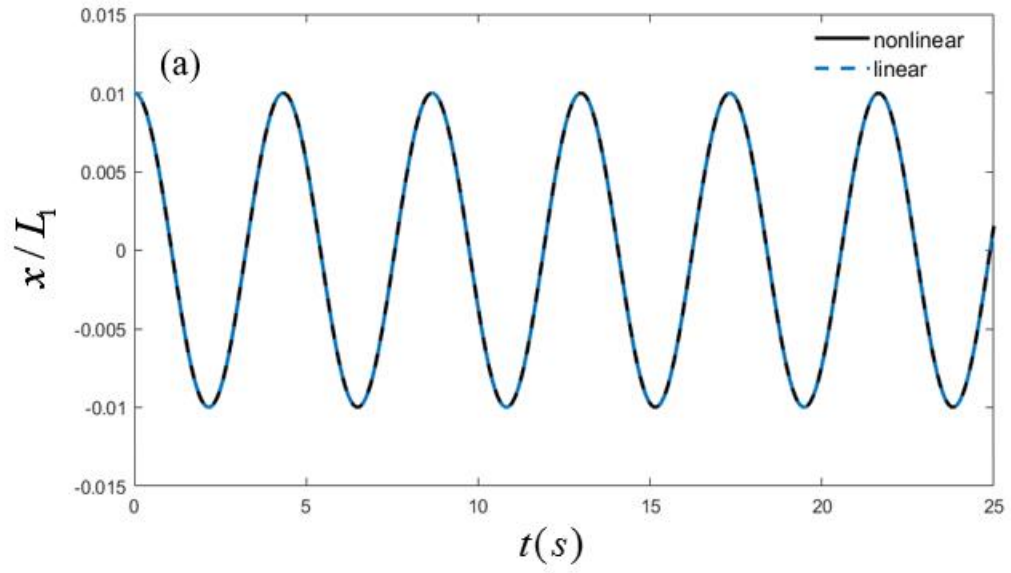
To illustrate the dynamic behavior of the DE oscillator under an external load, the frame of oscillator is excited with a displacement field  $y(t) = Y \cos(\omega_b t)$  (see figure 3-9), where  $Y$  is the amplitude of the excitation and  $\omega_b$  is the excitation frequency. Due to the external excitation, the absolute position of the rigid bar is changed to  $x = (\lambda_{1p} - \lambda_1) L_1 + y$ . Correspondingly, the equation of motion (3.17) is rewritten as,

$$\frac{d^2 \lambda_1}{dt^2} + a_1 \frac{d \lambda_1}{dt} + \frac{Y}{L_1} \omega_b^2 \cos(\omega_b t) + g(\lambda_1, \lambda_1^i, \lambda_2^i, V^*) = 0 \quad (3.21)$$



**Figure 3-9 Representation model of external excitation applied on an oscillator's frame**

Numerical solution of equation (3.21) gives the response of the oscillator according to the external base excitation. In order to ensure that the loss-of-tension does not occur, the pre-stretched ratio is selected as  $\lambda_{1p} = 4$  when high amplitude excitation is implemented. Figures 3-10 depicts the time response (displacement  $x / L_1$  versus time  $t$ ) of the rigid bar to the external excitation for both the linear and nonlinear models under a static voltage  $V^* = 0.1$ . In figure 3-10, for low frequency excitation  $\omega_b = 0.01\omega_n$  ((a) and (b)), the steady state response displacement amplitude is approximately the same as the excitation amplitude ((a)  $Y = 0.01L_1$  (b)  $Y = 1L_1$ ). However, for high excitation frequency  $\omega_b = 1.5\omega_n$  ((c) and (d)), the response amplitude is attenuated. Furthermore, simulation results from the two viscosity models stay almost the same at both transient and steady state. It is thus concluded that the displacement transmissibility is only frequency dependent.



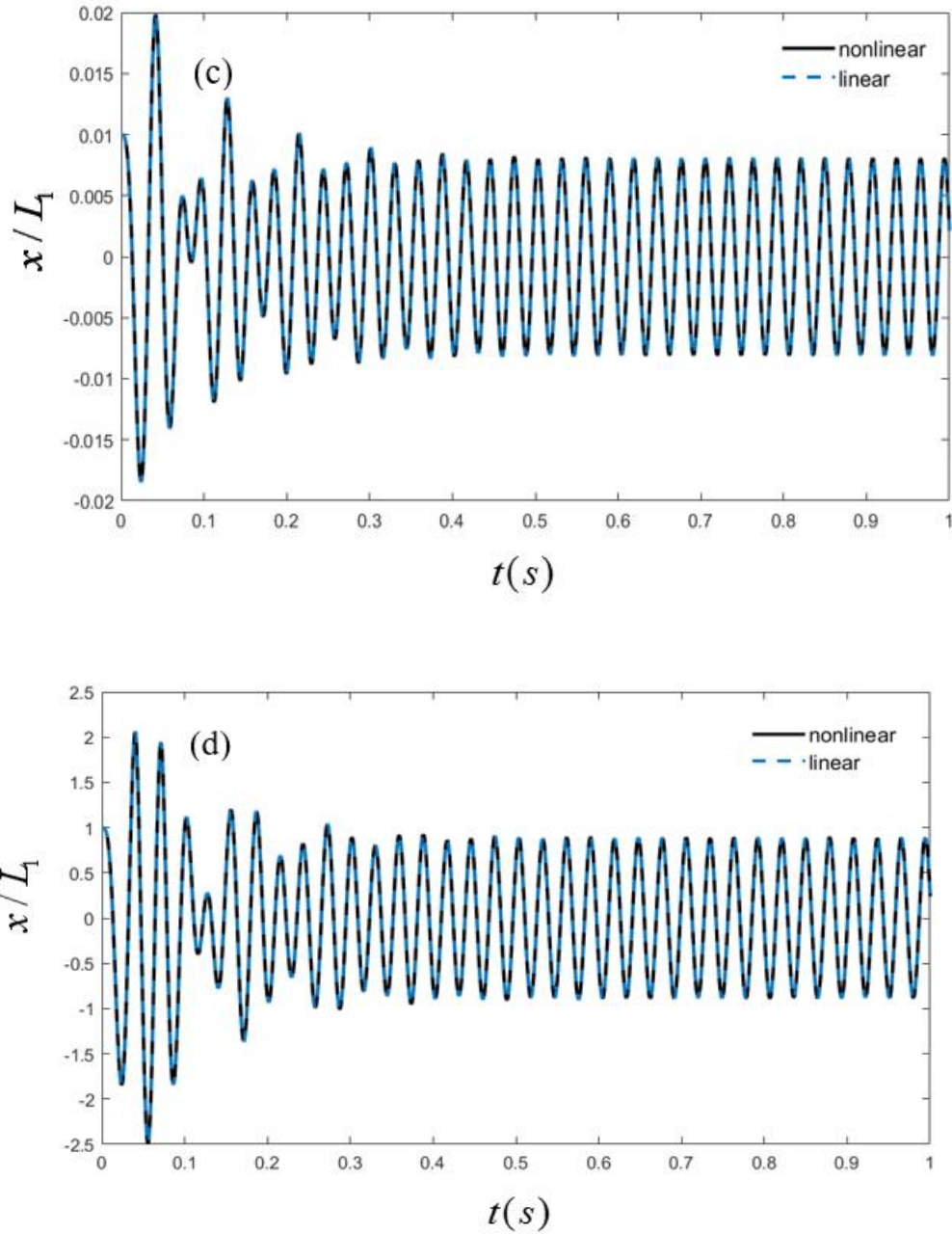


**Figure 3-10 Time response of the DE membrane oscillator under external excitation. The excitation frequency  $\omega_b$  varies between  $0.01\omega_n$  ((a) and (b)) and  $1.5\omega_n$  ((c) and (d)). The amplitude of excitation  $Y$  varies between  $0.01L_1$  ((a) and (c)) and  $1L_1$  ((b) and (d)).**

### 3.5 Conclusion

Based on the theory of finite deformation viscoelasticity and the coupled field theory for DEs, this work investigates the effect of nonlinear viscosity of material on the frequency tuning of a viscoelastic DE membrane oscillator, as well as its oscillation behavior under an AC voltage. Comparison of modeling the oscillation between a nonlinear viscosity model and a linear viscosity model shows that neglecting the deformation-dependent viscosity may lead to error in predicting the transient state response of the oscillator. Moreover, by investigating the time response of an oscillator to external base excitation, it can be concluded that the effect of nonlinear viscosity is negligible. The modeling framework and simulation results are anticipated to provide an increased understanding on the dynamic performance of vibrational dielectric elastomer devices.

## Chapter 4

### 4 The effect of nonlinear viscosity on the performance of dielectric elastomer energy generators

Dielectric elastomer generators (DEGs) are capable of converting mechanical energy from a variety of sources into electrical energy. The energy harvesting performance depends on the interplay between electromechanical coupling, material viscosity and multiple failure modes. Experiments also suggest that the material viscosity of dielectric elastomers is deformation dependent, which makes the prediction of the performance of DEGs more challenging. By adopting the coupled field theory, finite-deformation viscoelasticity theory and the theory for polymer dynamics, this work investigates the harvested energy and conversion efficiency of DEGs from theoretical perspective. By comparing the simulation results from the nonlinear viscosity model to the experimental data and the simulation results from the linear viscosity model, we further examine the possible factors that may strongly influence the performance of DEGs. It is found that DEGs exhibit higher harvested energy when nonlinear material viscosity is considered. Moreover, by selecting a higher voltage of the power supply for the generator, the conversion efficiency of DEGs can be greatly improved. The theoretical framework in this study is expected to offer some new insights into optimizing the design of DEGs and thus improving their performance

#### 4.1 Introduction

Dielectric elastomers (DEs) have drawn much attention in the field of transduction technology recently due to their high energy density, light weight, flexibility, and large deformation capability. DEs are particularly promising candidates used for harvesting energy from various sources including human motions, ocean waves, and wind (Kornbluh et al., 2012). Most dielectric elastomer generators (DEGs) can be envisaged as a DE membrane coated with compliant electrodes on its surfaces, which functions as variable capacitor to collect and transfer electrical charges during an energy harvesting process. First, the DE membrane is connected to a power source and stretched by external

mechanical forces, which increases the capacitance of the DE and force the charges to flow from the power supply to the compliant electrodes on the DE surfaces. Then the DE is disconnected from the power supply and allowed to shrink back to its original shape by releasing the applied mechanical forces. During this step the voltage on the DE increases due to the decrease of its capacitance, which enables the charge flow from DE capacitor to the storage. Through this electromechanical cycle, mechanical energy is converted into electrical energy. The amount of energy transferred depends on the change of the capacitance of the DE membrane. Based on this energy harvesting mechanism, DE generators with various configurations and harvesting schemes have been developed in the literature. One of the pioneering studies was conducted by Pelrine et al. (2001) by proposing a DEG with constant voltage scheme. The prototype developed by using acrylic elastomers could achieve energy density up to 400 J/kg. McKay et al. (2010) developed a self-priming DEG system in order to retain the charge losses and experimentally demonstrated the energy density ranging from 2.8 J/kg to 12.6 J/kg and the harvesting efficiency up to 84% for. Chiba et al. (2008) built a DEG aiming to collect energy from ocean waves, which was capable of generating 50W with wave height of 0.5m. Liu et al. (2010) designed stacking energy harvesters based on silicon elastomers to collect energy from water with energy density of 3.6J/kg. Koh et al. (2009) theoretically analyzed the maximal energy that can be converted by a DEG with the consideration of various failure modes, including electrical breakdown, electromechanical instability, loss of tension and rupture. Recently, more efforts have been devoted to improving the energy density or harvested efficiency of DEGs. For example, Huang et al. (2013) boosted the DEGs energy density to 560J/kg by adopting equi-biaxial loading that maximize change of the capacitance. A triangular energy harvesting scheme was proposed by Shian et al. (2014) to optimize the electromechanical harvesting cycle of a DEG which demonstrated the energy density could be up to 780J/kg. However, it should be mentioned that the energy harvesting performance of the DEGs, including energy density and conversion efficiency, is quite scattered in the literature. The currently obtained maximum energy density in the literature is still much lower than the theoretical prediction which could be as high as 1700 J/kg (Koh et al., 2011a).



One of the main factors that affect the harvesting performance of DEGs is the material viscoelasticity, which could cause high energy dissipation and loss-of-tension of membrane (Fan et al., 2018; Huang et al., 2013; Shian et al., 2014). Recently, based on the fully coupled field theory for DEs developed by Suo et al. (2008) and the finite-deformation viscoelasticity theory developed by Reese and Govindjee (1998), Hong (2011) has proposed a novel constitutive model capable of capturing the finite-deformation viscoelastic response of DEs under electromechanical coupling. By using the Hong's model (Hong, 2011) and the constant voltage harvesting scheme, the energy harvesting performance of DEs has been investigated. For example, Li et al. (2012b) have analyzed the inhomogeneous viscoelastic deformation of DEGs and the effect of rapid loading and unloading on the performance of DEGs. Foo et al. (2012b) studied the dissipative processes and current leakage in the harvesting cycle of DEGs. Zhou et al. (2015) investigated the energy density and the conversion efficiency of DEGs with their fatigue life taken into account. Chen et al. (2016) investigated the effect of temperature on the dissipative process of DEGs. A triangular harvesting scheme has also been explored to investigate energy harvesting performance of viscoelastic DEGs. For example, Zhou et al. (2017) developed a theoretical framework for analyzing the energy harvesting process of DEGs and proposed optimization methods to improve the energy harvesting performance. Fan et al. (2018) investigated the effect of loss-of-tension on energy harvesting performance of DEGs.

It should be mentioned that most existing studies about DEGs assume linear material viscosity within the framework of the finite-deformation viscoelasticity. In other words, the material viscosity is assumed as a constant in these studies. However, according to the theory of polymer dynamics (Doi and Edwards, 1988), the viscosity of the polymer chains in elastomers should not be a constant number, i.e. deformation-dependent, especially when they undergo large deformation. This argument has also been proven by physical experiments (Hossain et al., 2012; Wang et al., 2016). The effects of such nonlinear viscosity on the energy harvesting performance of DEGs have not been investigated thus far. Until recently, Zhou et al. (2018) has developed a constitutive law for elastomers that incorporated nonlinear viscosity of polymer chain into finite-deformation viscoelasticity theory, which is expected to better capture the time-dependent and rate-dependent deformation of DEs. In this work, the modeling framework by Zhou et al. (2018) will be

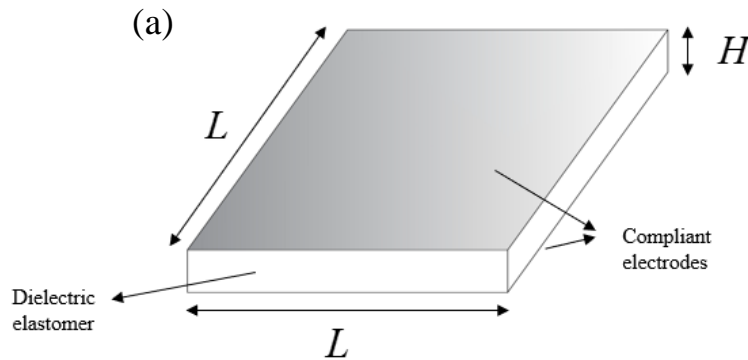
further employed to study the energy harvesting performance of DEGs with the triangular harvesting scheme. Particularly, the influence of the deformation-dependent viscosity on the energy density and conversion efficiency of the DEGs will be explored.

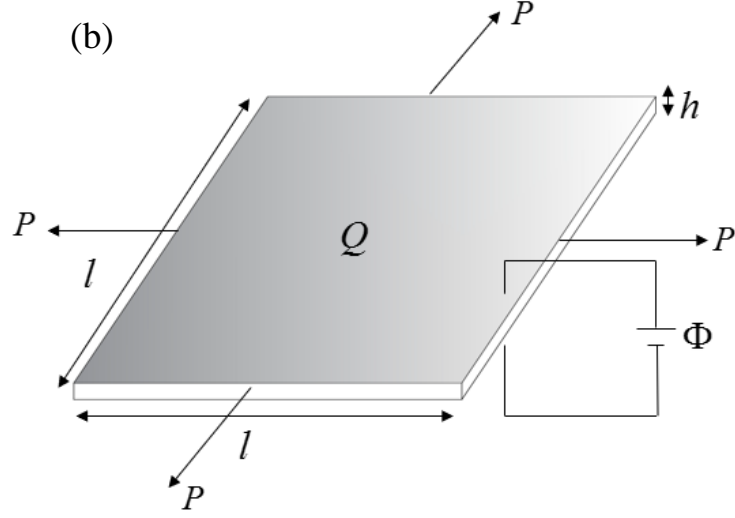
## 4.2 Model and Formulation

Figure 4-1 sketches the deformation process of the embedded DE membrane in the generator, which is covered by compliant electrodes on its top and bottom surfaces. The undeformed state is denoted by in-plane length  $L$  and thickness  $H$  as shown in (a). When the membrane is subjected to a voltage  $\Phi$  between the electrodes and equi-biaxial stretching force  $P$ , it deforms to the current state with length  $l$  and thickness  $h$ . Assuming homogeneous deformation and material incompressibility, the stretch ratios in-plane and along the thickness direction are defined as  $\lambda=l/L$  and  $\lambda_h=h/H$  with  $\lambda_h=1/\lambda^2$ . The applied voltage across the DE membrane also induces the charges accumulated on the two electrodes, i.e.,

$$\pm Q = C_{DE} \Phi, \quad (4.1)$$

where  $C_{DE} = \varepsilon \varepsilon_0 \lambda^4 L^2 / H$  is the capacitance of the DE membrane capacitor with  $\varepsilon_0$  being the dielectric permittivity of the vacuum and  $\varepsilon$  being the relative dielectric constant of the DE. It is evident that the change of the capacitance is realized through the continuous deformation of the membrane during the energy harvesting cycle, which governs the energy conversion of the DEG.





**Figure 4-1 Schematics of a dielectric elastomer membrane embedded in a DEG. (a) reference state (b) current state with voltage  $\Phi$  and pre-stretch force  $P$  applied.**

Under the homogeneous deformation condition, the deformation gradient of the current state with respect to the undeformed state can be expressed in terms of the stretch ratios as

$$\mathbf{F} = \begin{bmatrix} \lambda & 0 & 0 \\ 0 & \lambda & 0 \\ 0 & 0 & \lambda_h \end{bmatrix}. \text{ As commonly treated in the literature (Chiang Foo et al., 2012b; Hong,}$$

2011; Zhou et al., 2014), the deformation gradient  $\mathbf{F}$  of the viscoelastic DE membrane is decomposed into an elastic component and an inelastic component in a multiplicative format, which gives

$$\mathbf{F} = \mathbf{F}^e \mathbf{F}^i, \quad (4.2)$$

$$\text{where } \mathbf{F}^i = \begin{pmatrix} \lambda^i & 0 & 0 \\ 0 & \lambda^i & 0 \\ 0 & 0 & \lambda_h^i \end{pmatrix} \text{ and } \mathbf{F}^e = \begin{pmatrix} \lambda^e & 0 & 0 \\ 0 & \lambda^e & 0 \\ 0 & 0 & \lambda_h^e \end{pmatrix} \text{ with superscripts 'e' and 'i' representing}$$

the elastic and inelastic parts, respectively. The material incompressibility of the DE ensures  $\lambda_h = 1/\lambda^2$ ,  $\lambda_h^e = 1/(\lambda^e)^2$  and  $\lambda_h^i = 1/(\lambda^i)^2$ .

Due to the work done by tensile forces  $P$  and voltage  $\Phi$ , the variation Helmholtz free

energy density  $w$  is expressed as,

$$L^2 H \frac{\partial W}{\partial \lambda} \delta \lambda = 2PL \delta \lambda + \Phi \delta Q. \quad (4.3)$$

Following Hong's model (Chiang Foo et al., 2012b; Hong, 2011; Zhou et al., 2017) the total Helmholtz free energy  $w$  of the deformed DE membrane consists of two parts, i.e.,  $W = W^{EQ}(\lambda, \Phi) + W^{NEQ}(\lambda^e)$ .  $W^{EQ}$  is the equilibrium Helmholtz free energy, which is associated with both the total deformation and applied electric voltage  $\Phi$ ;  $W^{NEQ}$  is the non-equilibrium Helmholtz free energy, which is only related to the elastic deformation. It is worth noticing that the electric field is assumed to be always in equilibrium as the electric field always reaches the equilibrium state much faster than the mechanical deformation (Hong, 2011). According to the work of Huang and Suo (2012), the equilibrium Helmholtz free energy density  $W^{EQ}$  takes the form

$$W^{EQ} = W_s(\lambda) + \frac{\epsilon \epsilon_0}{2} \left( \frac{\Phi}{H} \right)^2 \lambda^4, \quad (4.4)$$

where  $W_s(\lambda)$  is the strain energy density function of the elastomer, and the second term is the free energy associated with the electric polarization. The finite deformation of elastomers has been well studied in the literature with hyperelastic constitutive models. Here, the Gent model (Gent, 1996) is adopted for case study to define the strain energy density function for both the equilibrium and the non-equilibrium parts, i.e.,

$$W_s = -\frac{G^{EQ} J_{\text{lim}}^{EQ}}{2} \ln \left( 1 - \frac{2\lambda^2 + \lambda^{-4} - 3}{J_{\text{lim}}} \right) \quad (4.5)$$

$$W^{NEQ} = -\frac{G^{NEQ} J_{\text{lim}}^{NEQ}}{2} \ln \left( 1 - \frac{2(\lambda^e)^2 + (\lambda^e)^{-4} - 3}{J_{\text{lim}}} \right), \quad (4.6)$$

where material constants  $J_{\text{lim}}^{EQ}$  and  $J_{\text{lim}}^{NEQ}$  are related to the total stretching limit and the stretching limit of the elastic component of the DE chains, respectively;  $G^{EQ}$  is the equilibrium shear modulus and  $G^{NEQ}$  is the non-equilibrium shear modulus.

Considering that  $\delta \lambda$  is any arbitrary small variation, substituting equations (4.4) -

(4.6) into (4.3) leads to

$$\frac{P}{GLH} = \frac{\chi J_{\text{lim}}^{EQ} (\lambda - \lambda^{-5})}{J_{\text{lim}}^{EQ} - 2\lambda^2 - \lambda^{-4} + 3} + \frac{(1-\chi) J_{\text{lim}}^{NEQ} (\lambda(\lambda^i)^{-2} - \lambda^{-5}(\lambda^i)^4)}{J_{\text{lim}}^{NEQ} - 2\left(\frac{\lambda}{\lambda^i}\right)^2 - \left(\frac{\lambda}{\lambda^i}\right)^{-4} + 3} - \frac{\varepsilon\varepsilon_0}{G} \left(\frac{\Phi}{H}\right)^2 \lambda^3, \quad (4.7)$$

where a new parameter  $\chi = G^{EQ} / G$  ( $0 \leq \chi \leq 1$ ) with  $G = G^{EQ} + G^{NEQ}$  is introduced to indicate the fraction of the time-independent polymer networks related to the total deformation (Bergström and Boyce, 1998). For limiting cases,  $\chi = 1$  represents a pure elastic medium, while  $\chi = 0$  is for a Newtonian fluid.

Since the free energy of the system never increases, the inelastic stretch ratio ( $\lambda^i$ ) in equation (4.7) must satisfy the thermodynamic evolution law (Hong, 2011; Reese and Govindjee, 1998), i.e.,

$$-\frac{1}{2} \mathbf{F} \frac{d\left[(\mathbf{C}^i)^{-1}\right]}{dt} \mathbf{F}^T (\mathbf{b}^e)^{-1} = \boldsymbol{\gamma}^{-1} : \boldsymbol{\tau}_{NEQ}, \quad (4.8)$$

Where  $\mathbf{C}^i = (\mathbf{F}^i)^T \mathbf{F}^i$ ,  $(\mathbf{b}^e)^{-1} = (\mathbf{F}^e)^T \mathbf{F}^e$ ,  $\boldsymbol{\tau}_{NEQ} = 2\mathbf{F}^e \frac{\partial W^{NEQ}}{\partial \mathbf{C}^e} (\mathbf{F}^e)^T$ ,  $\mathbf{C}^e = (\mathbf{F}^e)^T \mathbf{F}^e$  and  $\boldsymbol{\gamma}^{-1}$  is an isotropic rank four tensor. According to Reese's work (Reese and Govindjee, 1998),  $\boldsymbol{\gamma}^{-1}$  takes the form

$$\boldsymbol{\gamma}^{-1} = \frac{1}{2\eta} \left( \mathbf{I}^4 - \frac{1}{3} \mathbf{I} \otimes \mathbf{I} \right), \quad (4.9)$$

where  $\mathbf{I}^4 = \frac{1}{2} (\delta_{ik} \delta_{jl} + \delta_{il} \delta_{jk})$  is the fourth order symmetric identity tensor,  $\mathbf{I}$  is the second order identity tensor, and  $\eta$  represents the shear viscosity. According to this thermodynamic evolution law, the time dependent inelastic stretch ratios are expressed as

$$\frac{d\lambda^i}{dt} = \frac{G^{\text{NEQ}} J_{\text{lim}}^{\text{NEQ}} \lambda^i}{6\eta \left[ J_{\text{lim}} - 2 \left( \frac{\lambda}{\lambda^i} \right)^2 - \left( \frac{\lambda}{\lambda^i} \right)^{-4} + 3 \right]} \left[ \left( \frac{\lambda}{\lambda^i} \right)^2 - \left( \frac{\lambda}{\lambda^i} \right)^{-4} \right]. \quad (4.10)$$

In order to demonstrate the effect of current leakage on harvesting efficiency, the charge  $Q$  on DE is described as

$$\frac{dQ}{dt} = i - i_{\text{leak}}, \quad (4.11)$$

where  $i$  is the current through the conducting wire attached to the compliant electrodes on DE, and the leakage current  $i_{\text{leak}}$  is governed by an empirical exponential function (Chiang Foo et al., 2012b; Di Lillo et al., 2011).

$$i_{\text{leak}} = \sigma_0 e^{(E/E_0)} EL^2 \lambda^2. \quad (4.12)$$

Here  $\sigma_0$  is the conductivity of DE at low electric field,  $E_0 = 4 \times 10^7$  is an empirical material constant, and the electric field is governed by  $E = \Phi \lambda^2 / H$ . The time dependent quantities  $P, i, i_{\text{leak}}, \lambda^i, Q$ , and  $\Phi$  can be obtained by solving a set of differential-algebraic equations, i.e., equations (4.1), (4.7), and (4.10)-(4.12) when initial conditions are given.

It should be noted that  $\eta$  is the viscosity of the material in the current state, which depends on the deformation of the DE and should be constitutively prescribed to obtain the inelastic stretch ratios as shown in equation (4.10). Here, the theory of polymer dynamics by Doi and Edwards (1988) is adopted to determine the deformation-dependent viscosity. The details of this theory are well elaborated in the literature (Doi and Edwards, 1988; Zhou et al., 2018). The basic idea of this theory is that the motion of polymer chains is confined by the surrounding polymer chains. This topological constraint can be modeled by a tube-like region with the tube axis C-D defined as the primitive chain (figure 4-2 (a)). The viscosity of elastomers originates from the diffusion of the polymer chains in the material. For this model, the tube diameter is a function of the primitive length  $L$  of the polymer chain and the end-to-end vector  $\mathbf{R}$  of the of the primitive chain, i.e.,

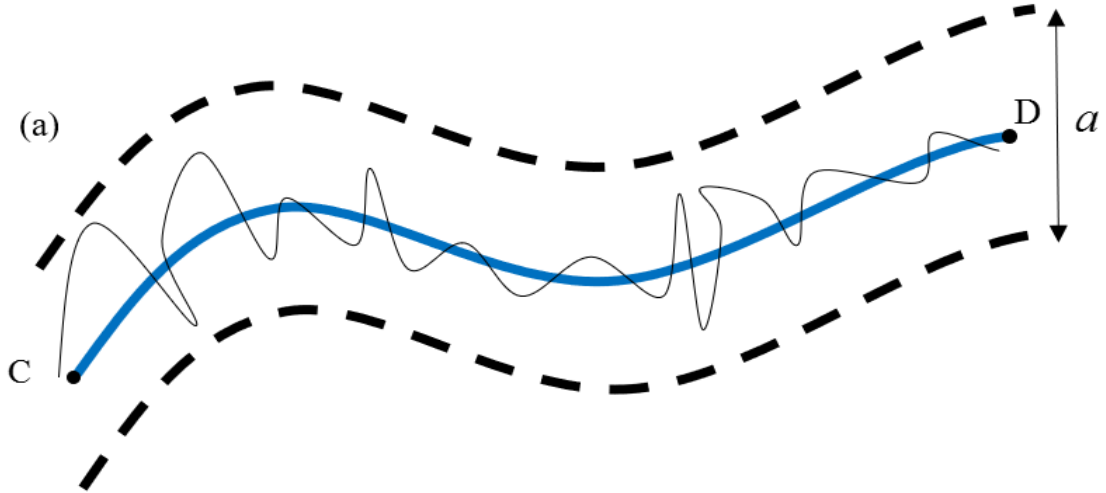
$\langle a \rangle = \langle \mathbf{R}^2 \rangle / \langle L \rangle$  with  $\langle * \rangle$  being the expectation operator of a parameter. It is easily perceived that both  $L$  and  $\mathbf{R}$  vary with the macroscopic deformation of the polymer, particularly when the DE undergoes large deformation with respect to the current state (figure 4-2 (b)). Therefore, the expectation of  $L$  and  $\mathbf{R}$  is a function of the deformation gradient  $\mathbf{F}$  and the statistical distribution function  $f_0(\mathbf{R})$  of the end-to-end vector, i.e.,

$\langle L \rangle = \int \frac{|\mathbf{F} \cdot \mathbf{u}|}{4\pi} L d^2 u$  and  $\langle \mathbf{R}^2 \rangle = \int |\mathbf{F} \cdot \mathbf{R}|^2 f_0(\mathbf{R}) d^3 R$  with  $\mathbf{u}$  being the unit tangent vector at a contour position of the polymer chain in the current state. The nonlinear viscosity was given by Doi and Edwards (1988) as,

$$\frac{\eta}{\eta_0} = \frac{a_0^2}{\langle a \rangle^2} = \frac{\left\langle \langle \mathbf{R}^2 \rangle_0 \frac{|\mathbf{F} \cdot \mathbf{u}|}{4\pi} d^2 \mathbf{u} \right\rangle^2}{\left\langle \int |\mathbf{F} \cdot \mathbf{R}|^2 f_0(\mathbf{R}) d^3 R \right\rangle}, \quad (4.13)$$

where  $a_0$  is the tube diameter and  $\eta_0 = \frac{1}{12} \frac{\zeta N^3 b_0^4 G_0}{k_b T a_0^2}$  is the viscosity in reference state. The

subscript “0” of the quantities refers to the reference state.



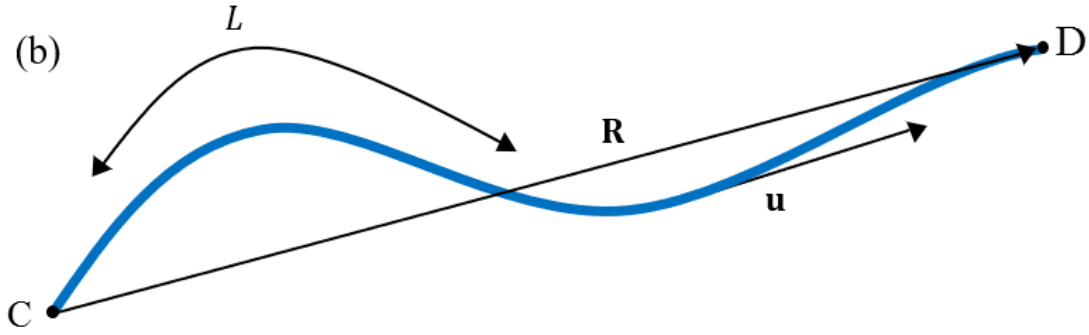


**Figure 4-2 (a) A tube-like region confines polymer chain C-D. The axis of the tube is the primitive chain of polymer chain C-D; (b) description of the primitive chain.**

### 4.3 Energy harvesting cycle of DEGs

The energy harvesting performance of the DEG with the triangular energy harvesting scheme (Shian et al. 2014) has been investigated by Zhou et al. (2017) using a linear viscosity model. Here the effect of nonlinear viscosity on their performance will be examined. In general, the achievable electrical energy is limited by the electromechanical integrity of the DE membrane, i.e., rupture and electrical breakdown. Therefore, a maximum stretch ratio  $\lambda_{\max}$  is first prescribed in order to prevent the DE from rupture. Meanwhile, a minimum stretch ratio  $\lambda_{\min}$  is usually prescribed as greater than 1 for the DE since it takes a longer time for the DE to recover back to the undeformed state during the energy harvesting cycle. When the applied voltage exceeds the breakdown voltage  $\Phi_B$  of the DE, the energy harvesting process will also fail due to the short-circuiting (Liu et al., 2012; Liu et al., 2009). The electrical breakdown voltage follows the rule of  $\Phi_B = E_B(1)H\lambda^{x-2}$  according to experiments (Huang et al., 2012), where  $E_B(1) = 30$  MV/m for the dielectric strength of the undeformed DE and  $x=1.13$  are determined through experimental data fitting. Acrylic elastomer VHB4905 is selected as the DE material for simulation, and the corresponding geometric and material parameters are set as  $L = 3.5\text{cm}$ ,  $H = 0.5\text{mm}$ ,  $\lambda_{\min} = 2$ ,  $\lambda_{\max} = 5.5$ ,  $\rho = 960\text{kg/m}^3$ ,  $\chi = 0.5$ ,  $\varepsilon = 4$ ,  $\varepsilon_0 = 8.85 \times 10^{-12}\text{F/m}$ ,  $G = 350\text{kPa}$ ,  $J_{\lim}^{\text{EQ}} = 110$ ,  $J_{\lim}^{\text{NEQ}} = 55$ , and the relaxation time  $\tau_0 = \frac{\eta_0}{G^{\text{NEQ}}} = 3$  in the



reference state (Chiang Foo et al., 2012a; Huang et al., 2013; Shian et al., 2014; Zhou et al., 2017).

In order to demonstrate the achievable harvested energy during the DEG harvesting cycle process, Figure 4-3(a) depicts the electrical breakdown,  $\lambda_{\max}$  and  $\lambda_{\min}$  curves of the embedded DE membrane on the charge-voltage work-conjugate plane following the work of Koh et al. (2011a). Theoretically, the maximum achievable energy during a harvesting cycle of the DEG is the area enclosed by these three curves. It is very difficult, if not impossible, to harvest the maximum energy due to the implementation feasibility of the energy harvesting scheme. However, a desirable harvesting cycle should be designed to cover this area as much as possible. Shian et al. (2014) have proposed a triangular harvesting cycle denoted by A-B-C in figure 4-3 (a), which appears to be capable of achieving as much energy as possible when the voltage at point B and the slope of BC are appropriately selected. The implementation of this harvesting scheme is relatively simple and could be realized by the electric circuit as shown in figure 4-3 (b). However, due to the material viscoelasticity of the DE, it requires extra time for the DEG to finish such a cycle A-B-C, which may lead to high energy dissipation and low efficiency. This triangular cycle was modified to A<sub>1</sub>-B<sub>1</sub>-C<sub>1</sub>-D<sub>1</sub> in the experiment of Shian et al. (2014). In order to further improve the energy harvesting performance of the generator, Zhou et al. (2017) has proposed a harvesting cycle as A<sub>2</sub>-B<sub>2</sub>-C<sub>2</sub>-D<sub>2</sub> for further optimization. For this cycle, loss-of-tension and current leakage of the DE membrane are both avoided, and the detailed process is well documented in their work. However, the nonlinear viscosity of the polymer chains is ignored in both works, which may significantly affect the harvesting process. Therefore, a harvesting cycle denoted by A<sub>3</sub>-B<sub>3</sub>-C<sub>3</sub>-D<sub>3</sub> with the consideration of material nonlinear viscosity is proposed in this work. The harvesting cycle proposed here follows the same path as in the work of Zhou et al. (Zhou et al., 2017) and is controlled by the electric circuit (figure 4-3 (b)), which is described as follows. With both switches 1 and 2 open, the DE membrane is stretched to the prescribed maximum stretch ratio  $\lambda_{\max} = 5.5$  by an equi-biaxial force  $P$  (denoted by point A<sub>3</sub> in the figure). Then Switch 1 is closed, and charges flow from the power supply to the DE capacitor. During this charging process as identified by A<sub>3</sub>-B<sub>3</sub>, the voltage on the DE keeps rising until it reaches the level of the

power supply, which is set as  $\Phi_L=3000$  V for example. Starting from state B<sub>3</sub>, switch 1 is re-opened and the bi-axial force  $P$  is decreased to allow the DE to shrink back. During this process, the capacitance of the DE decreases, leading to the increase of the voltage on the DE. Once the voltage on the DE is higher than that on the transfer capacitor, charges accumulated on the DE capacitor will flow to the transfer capacitor through the diode in the circuit. In order to achieve the maximum energy, it is expected to shrink the DE back to the prescribed minimum stretch, i.e., state C as originally proposed in the triangular scheme. However, it is found in the simulation that loss-of-tension of the DE membrane occurs during this process, which was also reported in the experiments by Shian et al. (2014) and the simulation by Zhou et al. (2017). In the experiment, the loss-of-tension was not avoided and the state C<sub>1</sub> is reached by the servomotor position. In the simulation, the loss-of-tension of the membrane is avoided by artificially selecting a state C<sub>3</sub> instead of state C. State C<sub>3</sub> is selected as the onset of the discharging process by closing switch 2, which allows the charges on both the DE and the transfer capacitors to flow to the harvesting circuit. This process continues until the DE membrane reaches a state of loss-of-tension at state D<sub>3</sub>, then the DE is immediately stretched again and switch 2 is reopened. Once the DE is stretched back to  $\lambda_{\max}$ , i.e., to state A<sub>3</sub>, the harvesting cycle is completed and will repeat. It should be noted that all the cycles presented in figure 4-3(a) are stable harvesting cycles after a few repeating cycles, which explains why A, A<sub>1</sub>, A<sub>2</sub> and A<sub>3</sub> do not start from the origin since there are residual charges from the previous cycle. The harvested energy is calculated by the area enclosed by A<sub>3</sub>-B<sub>3</sub>-C<sub>3</sub>-D<sub>3</sub> in our simulation as 0.5285 J and the energy density is determined as 873.73J/kg. Without considering the deformation-dependent viscosity, the harvested energy and the energy density were determined as 0.48 J and 794 J/kg, respectively (Zhou et al. 2017). It is found that the energy harvested through cycle A<sub>3</sub>-B<sub>3</sub>-C<sub>3</sub>-D<sub>3</sub> is more than the other two cycles A<sub>2</sub>-B<sub>2</sub>-C<sub>2</sub>-D<sub>2</sub> and A<sub>1</sub>-B<sub>1</sub>-C<sub>1</sub>-D<sub>1</sub> (0.47 J in the experiment by Shian et al. (2014))

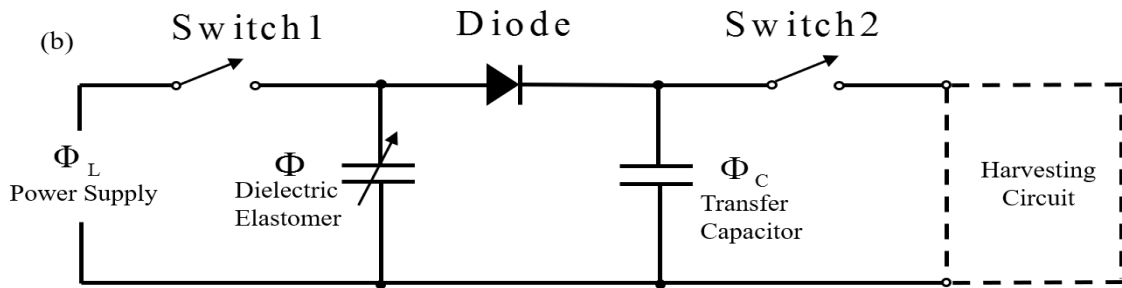
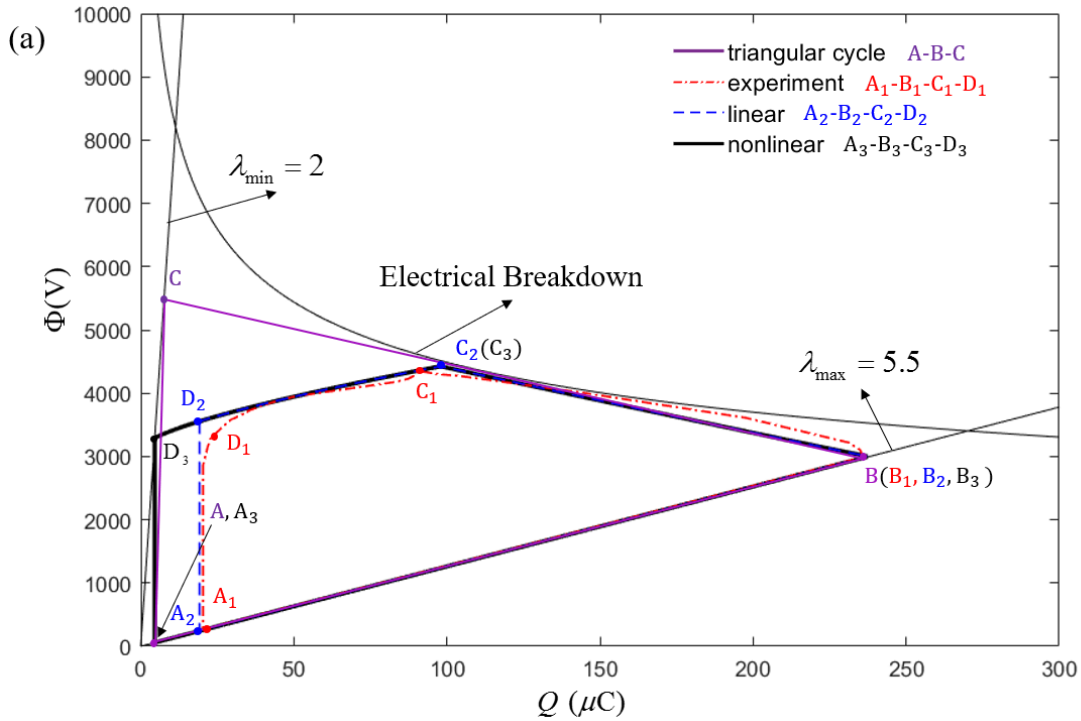
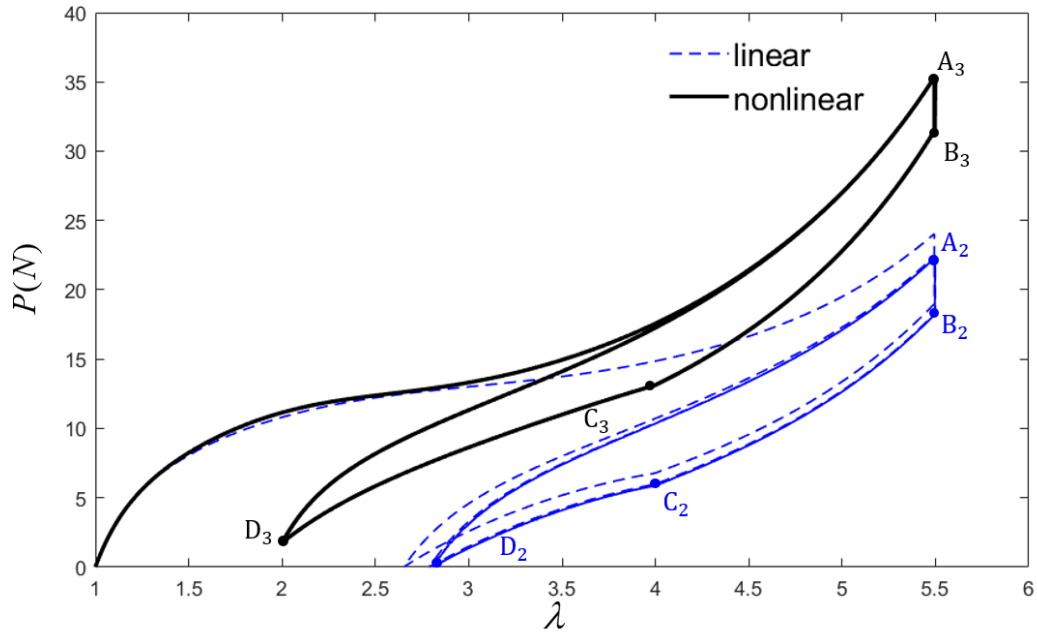


**Figure 4-3 Energy harvesting cycle of the DEG: (a) proposed triangular path, experimental path, simulation results by using both nonlinear and linear viscosity models; (b) circuit diagram used to control harvesting cycle.**

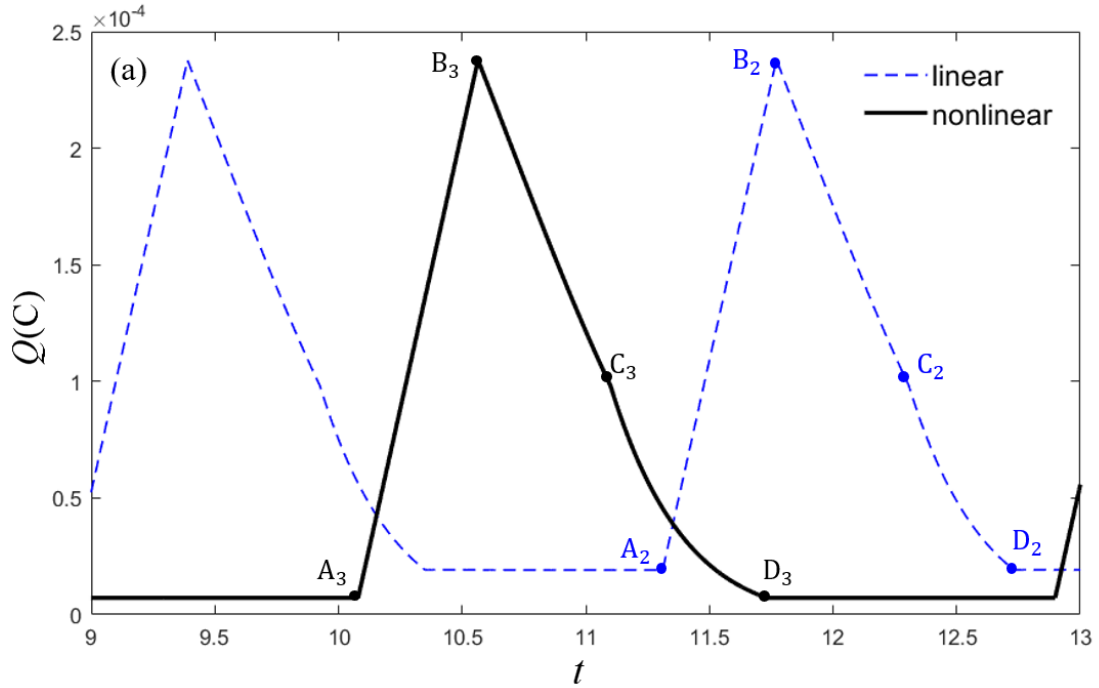
Figure 4-4 shows the force-stretch curve for both harvesting cycles  $A_2-B_2-C_2-D_2$  and  $A_3-B_3-C_3-D_3$ . Based on the experimental results of Shian et al (2014), where both the stretching and the shrinking rates are set as  $d\lambda/dt = 2.8s^{-1}$ . Meanwhile, the voltage of the DE ramps up at the rate of  $r_v = d\Phi/dt = 6000 \text{ V/s}$  during the charging process (from state  $A_2$  (or  $A_3$ ) to state  $B_2$  (or  $B_3$ )). It is found that it requires higher mechanical force to stretch the DE when the nonlinear material viscosity is considered. However, the electromechanical cycle for the nonlinear model reaches the steady state faster than the linear model. The

mechanical work done by the equi-biaxial force  $P$  can be calculated as two times of the area enclosed by these curves, which are calculated as 0.8076J and 0.7072J for the nonlinear viscosity model and the linear viscosity model, respectively. Correspondingly, the energy conversion efficiency for these two cycles  $A_2$ - $B_2$ - $C_2$ - $D_2$  and  $A_3$ - $B_3$ - $C_3$ - $D_3$  are determined as 67% and 65.4%, respectively, which is much higher than 30% obtained in the experiment (Shian et al. 2014). The main reason for the efficiency improvement is that the loss-of-tension of the DE membrane is avoided in the simulation, which prevents a large amount of energy dissipates during the inelastic deformation of the DE. This is realized through shortening the discharging process, i.e., from state  $C_2$  (or  $C_3$ ) to state  $D_2$  (or  $D_3$ ). It should also be mentioned that the possible energy dissipation through friction, plastic deformation and the electric circuit will certainly contribute to the lower energy conversion efficiency in the experiment.

Although the discharging process is shortened in the simulation process, its effect on the harvested energy of DEG is negligible since most of the charges have been transferred out of the DE at state  $D_2$  (or  $D_3$ ). This is evidenced by figure 4-5 (a), which shows the variation of the electric charge throughout the whole energy harvesting cycle. It is demonstrated that at the end of the discharging, there are little residual charges left. The change of the electrical voltage during the energy harvesting process is shown in figure 4-5(b), which follows  $\Phi = \Phi_C + (\Phi_L - \Phi_C)(1 - e^{-t/0.45})$  during the discharging process (state  $C_2$  (or  $C_3$ )- $D_2$  (or  $D_3$ ) with  $\Phi_C$  being the voltage level at state  $C_2$  (or  $C_3$ ). At state  $A_2$  (or  $A_3$ ) the voltage of the DE is non-zero since there are still some charges left on the DE capacitor from the previous harvesting cycle. In comparison of the nonlinear and linear models, it is found that the nonlinear model exhibits lower residual voltage and charge than the linear model. It should be mentioned that the current leakage (figure 4-5 (c)) is calculated as  $7.7 \times 10^{-6} \text{C}$  during the whole harvesting cycle, which is negligible by comparing with the peak value of the charges on the DE as shown in figure 4-5 (a). This conclusion is in agreement with both the simulation (Zhou et al., 2017) and the experiment (Shian et al., 2013).



**Figure 4-4** The force-stretch curve of the DE membrane during the electromechanical harvesting cycle for different viscosity models.



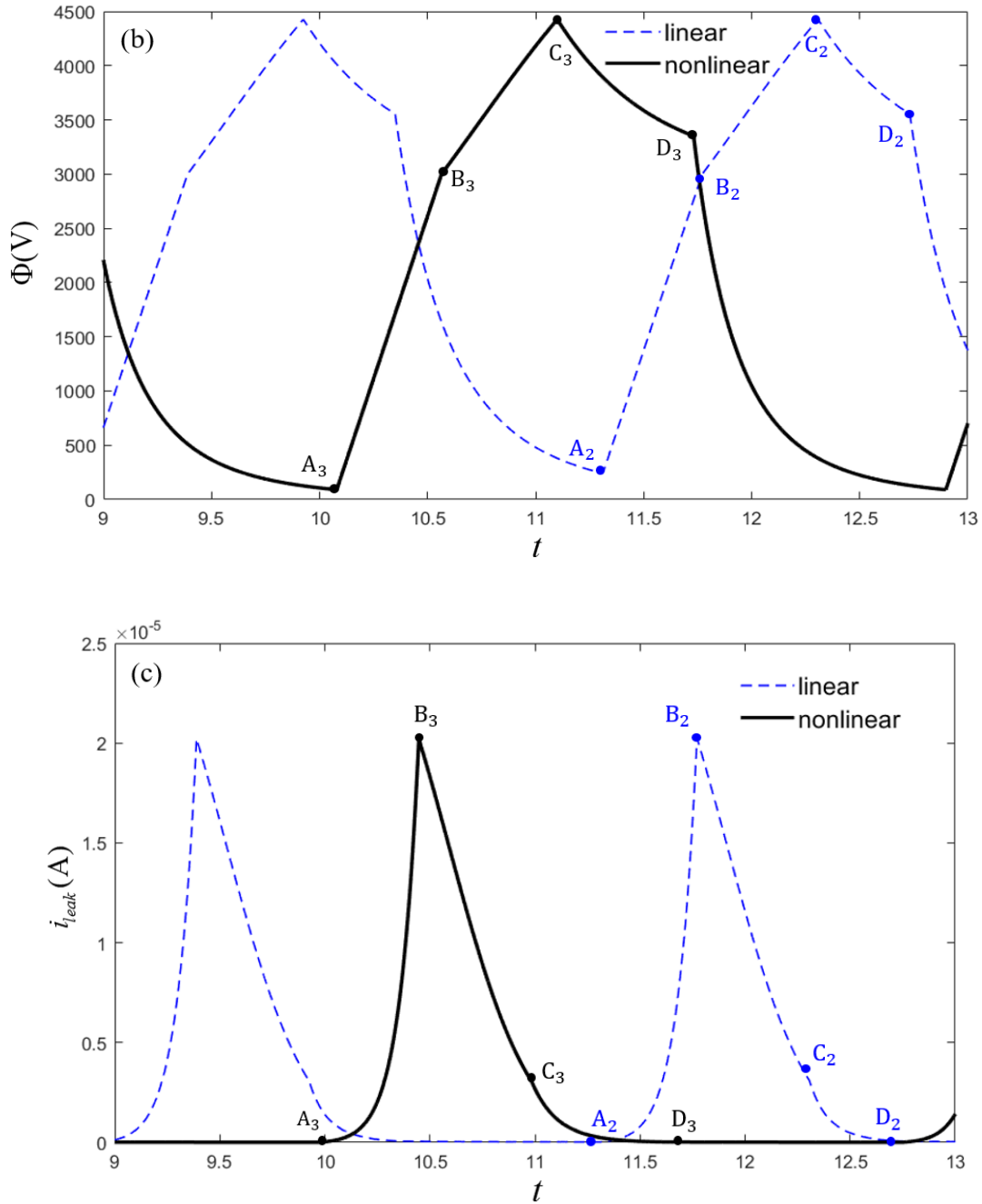


**Figure 4-5 The variation of charge (a), voltage (b) and current leakage (c) on the DE capacitor during the electromechanical harvesting cycle.**

From the above analysis, it can be concluded that the harvesting performance of the DEG, including the harvested energy and the conversion efficiency, is mainly governed by the voltage level of the power supply and the timing (or stretching state) for closing switch

2, i.e., the position of  $B_2$  (or  $B_3$ ) and  $C_2$  (or  $C_3$ ) on the energy harvesting curve. Therefore, a suitable combination of state  $B_3$  and  $C_3$  may help to improve the energy harvesting performance of the DEG, either the harvested energy, or the efficiency, or both. Figure 4-6 shows the variation of the harvested energy (figure 4-6 (a)) and the efficiency (figure 4-6 (b)) of the DEG with the stretch ratio at state  $C_3$  ( $\lambda_{C_3}$ ) and the voltage level of the power source ( $\Phi_L$ ) when the nonlinear material viscosity is considered. It is observed that both the harvested energy and the conversion efficiency increase when a higher power supply voltage  $\Phi_L$  and a lower stretch ratio  $\lambda_{C_3}$  are selected. This trend is different from the one predicted by the linear viscosity model (Zhou et al., 2017), which indicates the significance of considering nonlinear material viscosity in the modeling framework of the DE. Within the given range of the power supply voltage and the stretching ratio  $\lambda_{C_3}$  at  $C_3$ , the maximum energy can be harvested is 0.6 J and the highest conversion efficiency is 69%. It is thus concluded that choosing a higher power supply voltage and smaller  $\lambda_{C_3}$  (or delay of closing switch 2) is an effective approach to improve both the harvested energy and the efficiency of DEG. However, it should be ensured that the voltage level of the power source is lower than the electrical breakdown voltage of DE at  $B_3$ , and the loss-of-tension does not occur at state  $C_3$ .

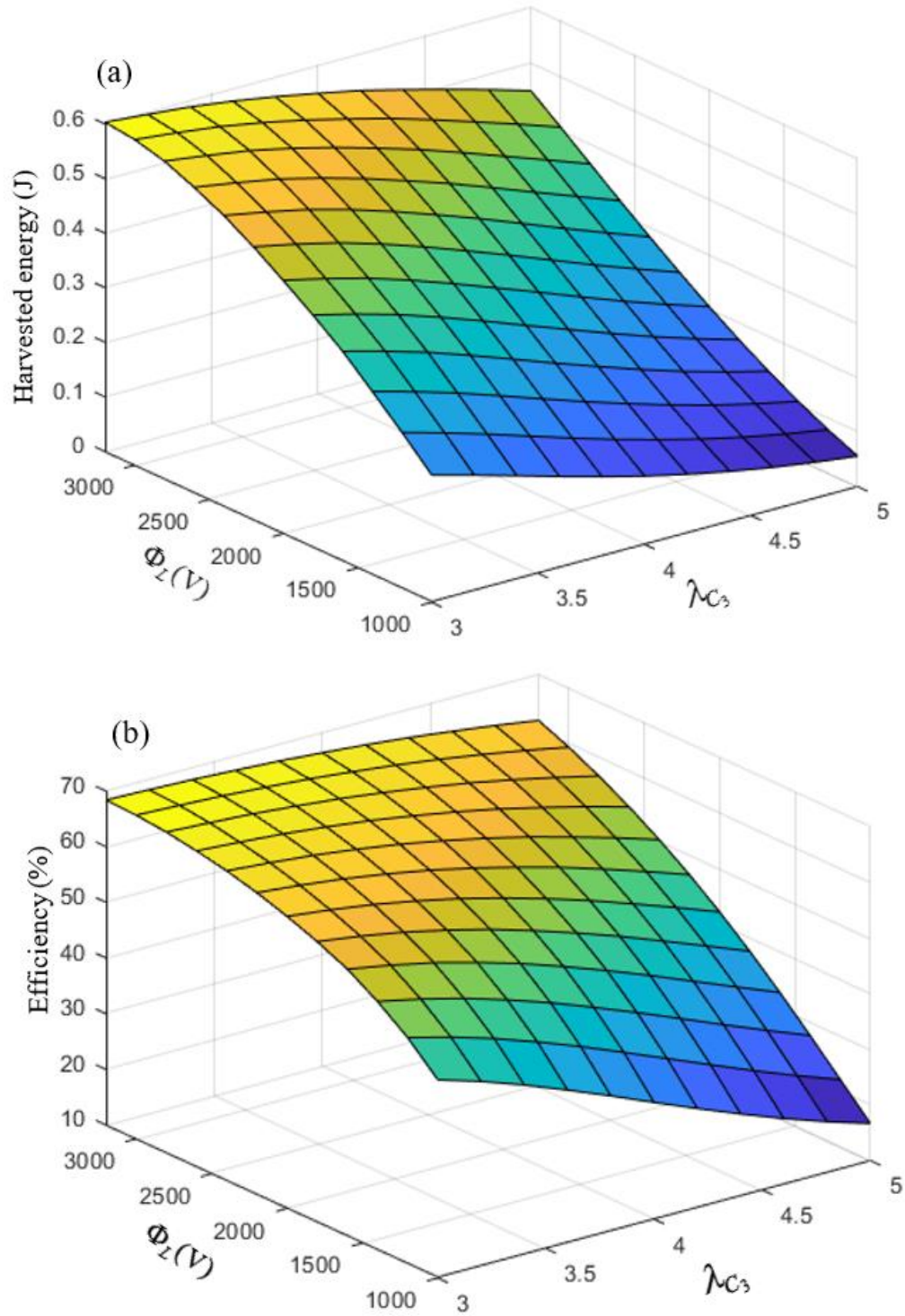


**Figure 4-6 Variation of harvested energy and efficiency DEG with the stretch ratio at  $C_3$  and the voltage level of power supply (a) harvesting energy (b) conversion efficiency.**



With the theoretical framework developed in the current work, we also evaluate the energy harvesting performance of DEGs with different types of polymer networks. Figure 4-7 depicts the maximum harvested energy and the maximum efficiency of a DEG as a function of  $\chi$  when the power supply voltage level  $\Phi_L$  is set as 3000 V. The results from the linear viscosity model by Zhou et al. (2017) are also plotted for comparison. It is observed that as  $\chi$  increases, the maximum harvested energy of the DEG increases until approaching a constant when  $\chi$  reaches a critical value for both models. This is expected since DE membranes with  $\chi$  higher than the critical value, they are able to shrink back to the prescribed minimum stretch ratio  $\lambda_{\min}=2$  without loss-of-tension, i.e., both  $C_2$  and  $C_3$  in the simulated harvesting cycles coincide with the originally proposed state C in the triangular scheme A-B-C. It is thus concluded that the ideal triangular harvesting scheme could be realized when the fraction of the time-independent polymer networks in the material is higher than this critical value. For the limiting case of a purely elastic solid with  $\chi=1$ , the maximum harvested energy is determined as 0.62 J when  $\Phi_L=3000$  V, which is quite close to the maximum achievable energy 0.74 J of the DEG as calculated by the enclosed area by the electrical breakdown,  $\lambda_{\max}$  and  $\lambda_{\min}$  curves in figure 4-3 (a). It is also found that the critical value of the fraction of time-independent polymer networks is different for the two models, e.g.,  $\chi=0.45$  for the nonlinear model and  $\chi=0.6$  for the linear model. On the other hand, the change of the maximum efficiency exhibits non-monotonic behavior, which attributes to the combined effect of the material viscoelasticity on the harvested energy and the mechanical work consumed during the harvesting cycle. This curve exhibits similar trend for both the linear and nonlinear viscosity models. While the discrepancy between the linear and nonlinear models indicates that neglecting the nonlinear behavior of the material viscosity may lead to significant error in analyzing the harvesting performance of DEGs.

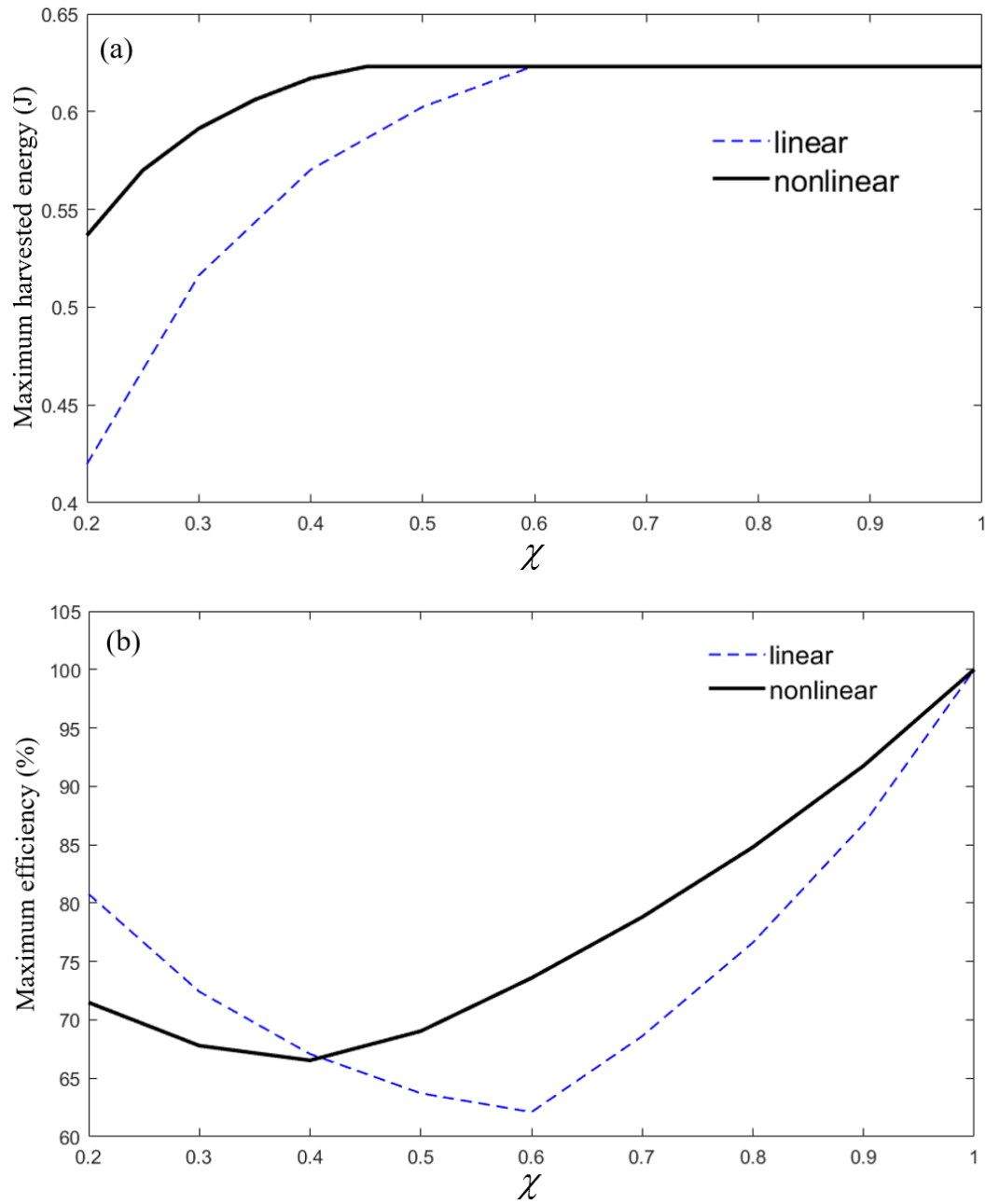


**Figure 4-7** Maximum harvested energy (a) and maximum efficiency (b) of DE in terms of material parameter  $\chi$ .

## 4.4 Conclusion

Based on the finite-deformation viscoelasticity theory and the theory of polymer dynamics, a theoretical framework with the consideration of material nonlinear viscosity is developed to comprehensively evaluate the energy harvesting performance of DEGs. Simulation results show that using a higher voltage power supply for energy harvesting is an effective way to improve both the harvested energy and the conversion efficiency of the DEG. Meanwhile, avoiding loss-of-tension of the DE membrane by shortening the discharging process in the energy harvesting cycle can significantly increase the conversion efficiency. This work also theoretically proves that the ideal triangular energy harvesting scheme could be realized by using DEs with higher fraction of time-independent polymer networks. Comparison between the linear and nonlinear models strengthens the significance of considering nonlinear material viscosity in modeling dielectric elastomers. This work aims to provide an increased understanding on how the deformation-dependent material viscosity affects the energy harvesting performance of DEGs and is expected to provide optimization guidance for further experimental works.

## Chapter 5

### 5 Conclusion and future work

#### 5.1 Contribution

Among the most promising electroactive polymers for transduction technologies, dielectric elastomers are featured with high flexibility, large deformation capability and high energy density compared to piezoelectric and electromagnetic materials. However, the performance of dielectric elastomers is affected by a few critical factors such as the nonlinear viscoelastic material nature, loading conditions and multiple failure modes. Extensive studies have been conducted on the viscoelastic effect of dielectric elastomers. Nevertheless, most of these studies assume linearity of the material viscosity, while experiments have confirmed that the material viscosity of DEs is highly nonlinear (deformation-dependent). Therefore, the objective of this work is to incorporate the deformation-dependent material viscosity into the finite-deformation viscoelasticity modeling framework with the consideration of multiple failure modes to investigate the viscoelastic effect on the performance of DE oscillators and generators. The models and results in this work are expected to provide guidelines for the optimal design of DE oscillators and generators. The contributions of this thesis include:

1. Incorporating the nonlinear viscosity into the finite-deformation viscoelasticity theory for dielectric elastomers, this work examines the natural frequency tuning process and the dynamic performance of DE oscillators under external excitation. To demonstrate the effect of nonlinear viscosity, comparisons of predictions for the frequency tuning, tunable frequency range and influence of electrical loading rate from the linear and nonlinear models are presented. In addition, the influence of nonlinear material viscosity on time response of DE resonator under external excitation was also examined.
2. With the deformation-dependent viscosity incorporated in the finite-deformation viscoelasticity model, this work also investigates the energy conversion efficiency, the harvested energy and the energy density of viscoelastic DE membrane

generators. To illustrate the effect of the nonlinear material viscosity on the energy harvesting process, comparisons of the harvested energy in an energy harvesting cycle, the variation of mechanical loads, and the maximum conversion efficiency predicted by the nonlinear and linear viscosity models are presented.

## 5.2 Conclusion remarks

According to our simulation results, some concluding remarks of this work are listed below:

1. It is found that, during the frequency tuning process, the nonlinear viscosity model predicts a faster relaxation than the linear model. Therefore, neglecting the nonlinear viscosity can lead to error in determining the natural frequency of DE-based vibration device.
2. Simulation results also show that the tuned natural frequency does not change with the voltage loading rate. Moreover, the applied voltage should be maintained below the electrical breakdown voltage of the DE.
3. For viscoelastic DE generators, it requires higher mechanical force to stretch DE when the nonlinear viscosity is considered. However, the electromechanical cycle predicted by the nonlinear model reaches the steady state faster than the linear model.
4. It is also concluded that the conversion efficiency improvement in the simulation is mainly due to the fact that loss-of-tension of the DE membrane is avoided by connecting system to harvesting circuit earlier. This prevents a large amount of energy from dissipating during the inelastic deformation of the DE.

## 5.3 Future work

The results of this work are expected to provide guidelines for DE-based vibrational devices and dielectric elastomer energy harvesters. However, the proposed modeling framework is still limited in certain aspects. Consequently, there are some suggestions for our future work:

1. The finite-deformation viscoelasticity with consideration of nonlinear viscosity above is assumed to have one purely elastic ground network and only one type of viscous subnetwork. However, according to experimental results, DEs tend to have multiple relaxation processes, which should be captured by multiple viscous subnetworks. Therefore, there is still much room to improve the model to examine the comprehensive performance of DE oscillators and generators.
2. Moreover, the dielectric strength of DEs is considered constant in this work. Nevertheless, experiments suggest that the dielectric strength of DEs changes with some factors like temperature, pressure, and deformation. Therefore, it is also essential to develop a model to account for the effect of the varying dielectric strength, which could improve the accuracy of the prediction for the performance of DE-based devices.

## References

- Ahmadi, S., Gooyers, M., Soleimani, M., Menon, C., 2013. Fabrication and electromechanical examination of a spherical dielectric elastomer actuator. *Smart Materials and Structures* 22, 115004.
- Anderson, I.A., Hale, T., Gisby, T., Inamura, T., McKay, T., O'Brien, B., Walbran, S., Calius, E.P., 2010. A thin membrane artificial muscle rotary motor. *Applied Physics A* 98, 75.
- Ashley, S., 2003. Artificial muscles. *Scientific American* 289, 52-59.
- Bergström, J., Boyce, M., 1998. Constitutive modeling of the large strain time-dependent behavior of elastomers. *Journal of the Mechanics and Physics of Solids* 46, 931-954.
- Biggs, S.J., Hitchcock, R.N., 2010. Artificial muscle actuators for haptic displays: system design to match the dynamics and tactile sensitivity of the human fingerpad, *Electroactive Polymer Actuators and Devices (EAPAD) 2010*. International Society for Optics and Photonics, 76420I.
- Boyce, M.C., Weber, G., Parks, D.M., 1989. On the kinematics of finite strain plasticity. *Journal of the Mechanics and Physics of Solids* 37, 647-665.
- Carpi, F., De Rossi, D., Kornbluh, R., Pelrine, R.E., Sommer-Larsen, P., 2011. *Dielectric elastomers as electromechanical transducers: Fundamentals, materials, devices, models and applications of an emerging electroactive polymer technology*. Elsevier.
- Chen, S. E., Deng, L., He, Z. C., Li, E., & Li, G. Y., 2016. Temperature effect on the performance of a dissipative dielectric elastomer generator with failure modes. *Smart Materials and Structures*, 25(5), 055017.
- Chiang Foo, C., Cai, S., Jin Adrian Koh, S., Bauer, S., Suo, Z., 2012a. Model of dissipative dielectric elastomers. *Journal of Applied Physics* 111, 034102.
- Chiang Foo, C., Jin Adrian Koh, S., Keplinger, C., Kaltseis, R., Bauer, S., Suo, Z., 2012b. Performance of dissipative dielectric elastomer generators. *Journal of Applied Physics* 111, 094107.
- Chiba, S., Waki, M., Kornbluh, R., Pelrine, R., 2008. Innovative power generators for energy harvesting using electroactive polymer artificial muscles, *Electroactive Polymer Actuators and Devices (EAPAD) 2008*. International Society for Optics and Photonics, 692715.
- Coleman, B.D., Gurtin, M.E., 1967. Thermodynamics with internal state variables. *The Journal of Chemical Physics* 47, 597-613.

- Christensen, R. M., 1980. A nonlinear theory of viscoelasticity for application to elastomers. *Journal of Applied Mechanics*, 47(4), 762-768.
- de Gennes, P.-G., 1971. Reptation of a polymer chain in the presence of fixed obstacles. *The journal of chemical physics* 55, 572-579.
- Di Lillo, L., Schmidt, A., Bergamini, A., Ermanni, P., Mazza, E., 2011. Dielectric and insulating properties of an acrylic DEA material at high near-DC electric fields, *Electroactive Polymer Actuators and Devices (EAPAD) 2011*. International Society for Optics and Photonics, 79763B.
- Doi, M., Edwards, S.F., 1988. *The theory of polymer dynamics*. oxford university press.
- Dorfmann, A., Ogden, R., 2005. Nonlinear electroelasticity. *Acta Mechanica* 174, 167-183.
- Fan, P., Chen, H., Li, B., Wang, Y., 2018. Performance investigation on dissipative dielectric elastomer generators with a triangular energy harvesting scheme. *EPL (Europhysics Letters)* 120, 47007.
- Feng, C., Jiang, L., Lau, W.M., 2011. Dynamic characteristics of a dielectric elastomer-based microbeam resonator with small vibration amplitude. *Journal of Micromechanics and Microengineering* 21, 095002.
- Gent, A., 1996. A new constitutive relation for rubber. *Rubber chemistry and technology* 69, 59-61.
- Goulbourne, N., Mockensturm, E., Frecker, M., 2005. A nonlinear model for dielectric elastomer membranes. *Journal of Applied Mechanics* 72, 899-906.
- Ha, S.M., Yuan, W., Pei, Q., Pelrine, R., Stanford, S., 2006. Interpenetrating polymer networks for high - performance electroelastomer artificial muscles. *Advanced Materials* 18, 887-891.
- Hong, W., 2011. Modeling viscoelastic dielectrics. *Journal of the Mechanics and Physics of Solids* 59, 637-650.
- Hossain, M., Vu, D.K., Steinmann, P., 2012. Experimental study and numerical modelling of VHB 4910 polymer. *Computational Materials Science* 59, 65-74.
- Huang, J., Shian, S., Suo, Z., Clarke, D.R., 2013. Maximizing the energy density of dielectric elastomer generators using equi - biaxial loading. *Advanced Functional Materials* 23, 5056-5061.
- Huang, R., Suo, Z., 2011. Electromechanical phase transition in dielectric elastomers. *Proceedings of the Royal Society A: Mathematical, Physical and Engineering Sciences* 468, 1014-1040.



- Huang, R., Suo, Z., 2012. Electromechanical phase transition in dielectric elastomers. *Proc. R. Soc. A* 468, 1014-1040.
- Jung, K., Kim, K. J., Choi, H. R. 2007. A self-sensing dielectric elastomer actuator. *Sensors and Actuators A: Physical*. Volume 143, Issue 2, 16 May 2008, 343-351.
- Keplinger, C., Kaltenbrunner, M., Arnold, N., Bauer, S., 2010. Röntgen's electrode-free elastomer actuators without electromechanical pull-in instability. *Proceedings of the National Academy of Sciences* 107, 4505-4510.
- Keplinger, C., Li, T., Baumgartner, R., Suo, Z., Bauer, S., 2012. Harnessing snap-through instability in soft dielectrics to achieve giant voltage-triggered deformation. *Soft Matter* 8, 285-288.
- Koh, S.J.A., Keplinger, C., Li, T., Bauer, S., Suo, Z., 2011a. Dielectric elastomer generators: How much energy can be converted? *IEEE/ASME Transactions on mechatronics* 16, 33-41.
- Koh, S.J.A., Li, T., Zhou, J., Zhao, X., Hong, W., Zhu, J., Suo, Z., 2011b. Mechanisms of large actuation strain in dielectric elastomers. *Journal of Polymer Science Part B: Polymer Physics* 49, 504-515.
- Koh, S.J.A., Zhao, X., Suo, Z., 2009. Maximal energy that can be converted by a dielectric elastomer generator. *Applied Physics Letters* 94, 262902.
- Kollosche, M., Zhu, J., Suo, Z., Kofod, G., 2012. Complex interplay of nonlinear processes in dielectric elastomers. *Physical Review E* 85, 051801.
- Kornbluh, R., Pelrine, R., Joseph, J., 1995. Elastomeric dielectric artificial muscle actuators for small robots, *Proceedings of the Third IASTED International Conference on Robotics and Manufacturing*, 14-16.
- Kornbluh, R.D., Pelrine, R., Pei, Q., Heydt, R., Stanford, S., Oh, S., Eckerle, J., 2002. Electroelastomers: applications of dielectric elastomer transducers for actuation, generation, and smart structures, *Smart Structures and Materials 2002: Industrial and Commercial Applications of Smart Structures Technologies*. International Society for Optics and Photonics, 254-271.
- Kornbluh, R.D., Pelrine, R., Pei, Q., Oh, S., Joseph, J., 2000. Ultrahigh strain response of field-actuated elastomeric polymers, *Smart Structures and Materials 2000: Electroactive Polymer Actuators and Devices (Eapad)*. International Society for Optics and Photonics, 51-65.
- Kornbluh, R.D., Pelrine, R., Prahlad, H., Wong-Foy, A., McCoy, B., Kim, S., Eckerle, J., Low, T., 2012. Dielectric elastomers: Stretching the capabilities of energy harvesting. *MRS bulletin* 37, 246-253.

- Löwe, C., Zhang, X., Kovacs, G., 2005. Dielectric elastomers in actuator technology. *Advanced engineering materials* 7, 361-367.
- Lee, E.H., 1969. Elastic-plastic deformation at finite strains. *Journal of applied mechanics* 36, 1-6.
- Leng, J., Liu, L., Liu, Y., Yu, K., Sun, S., 2009. Electromechanical stability of dielectric elastomer. *Applied Physics Letters* 94, 211901.
- Li, T., Qu, S., Yang, W., 2012a. Electromechanical and dynamic analyses of tunable dielectric elastomer resonator. *International Journal of Solids and Structures* 49, 3754-3761.
- Li, T., Qu, S., Yang, W., 2012b. Energy harvesting of dielectric elastomer generators concerning inhomogeneous fields and viscoelastic deformation. *Journal of Applied Physics* 112, 034119.
- Linder, C., Tkachuk, M., Miehe, C., 2011. A micromechanically motivated diffusion-based transient network model and its incorporation into finite rubber viscoelasticity. *Journal of the Mechanics and Physics of Solids* 59, 2134-2156.
- Liu, L., Liu, Y., Leng, J., 2012. Voltage-induced deformation in dielectric. *Journal of Applied Physics* 112, 033519.
- Liu, Y., Liu, L., Zhang, Z., Jiao, Y., Sun, S., Leng, J., 2010. Analysis and manufacture of an energy harvester based on a Mooney-Rivlin-type dielectric elastomer. *EPL (Europhysics Letters)* 90, 36004.
- Liu, Y., Liu, L., Zhang, Z., Leng, J., 2009. Dielectric elastomer film actuators: characterization, experiment and analysis. *Smart Materials and Structures* 18, 095024.
- McKay, T., O'Brien, B., Calius, E., Anderson, I., 2010. An integrated, self-priming dielectric elastomer generator. *Applied Physics Letters* 97, 062911.
- McMeeking, R.M., Landis, C.M., 2005. Electrostatic forces and stored energy for deformable dielectric materials. *Journal of Applied Mechanics* 72, 581-590.
- Miehe, C., Göktepe, S., Lulei, F., 2004. A micro-macro approach to rubber-like materials—part I: the non-affine micro-sphere model of rubber elasticity. *Journal of the Mechanics and Physics of Solids* 52, 2617-2660.
- O'Brien, B.M., Calius, E.P., Inamura, T., Xie, S.Q., Anderson, I.A., 2010. Dielectric elastomer switches for smart artificial muscles. *Applied Physics A* 100, 385-389.
- O'Halloran, A., O'malley, F., McHugh, P., 2008. A review on dielectric elastomer actuators, technology, applications, and challenges. *Journal of Applied Physics* 104, 9.

- Ogden, R.W., 1972. Large deformation isotropic elasticity—on the correlation of theory and experiment for incompressible rubberlike solids. *Proc. R. Soc. Lond. A* 326, 565-584.
- Park, H.S., Nguyen, T.D., 2013. Viscoelastic effects on electromechanical instabilities in dielectric elastomers. *Soft Matter* 9, 1031-1042.
- Pelrine, R., Kornbluh, R., Pei, Q., Joseph, J., 2000. High-speed electrically actuated elastomers with strain greater than 100%. *Science* 287, 836-839.
- Pelrine, R., Kornbluh, R.D., Eckerle, J., Jeuck, P., Oh, S., Pei, Q., Stanford, S., 2001. Dielectric elastomers: generator mode fundamentals and applications, *Smart Structures and Materials 2001: Electroactive Polymer Actuators and Devices*. International Society for Optics and Photonics, 148-157.
- Pelrine, R., Kornbluh, R.D., Pei, Q., Stanford, S., Oh, S., Eckerle, J., Full, R.J., Rosenthal, M.A., Meijer, K., 2002. Dielectric elastomer artificial muscle actuators: toward biomimetic motion, *Smart Structures and Materials 2002: Electroactive polymer actuators and devices (EAPAD)*. International Society for Optics and Photonics, 126-138.
- Pelrine, R.E., Kornbluh, R.D., Joseph, J.P., 1998. Electrostriction of polymer dielectrics with compliant electrodes as a means of actuation. *Sensors and Actuators A: Physical* 64, 77-85.
- Plante, J.-S., Dubowsky, S., 2006. Large-scale failure modes of dielectric elastomer actuators. *International journal of solids and structures* 43, 7727-7751.
- Plante, J.-S., Dubowsky, S., 2007. On the performance mechanisms of dielectric elastomer actuators. *Sensors and Actuators A: Physical* 137, 96-109.
- Pyckhout-Hintzen, W., Westermann, S., Wischnewski, A., Monkenbusch, M., Richter, D., Straube, E., Farago, B., Lindner, P., 2013. Direct observation of nonaffine tube deformation in strained polymer networks. *Physical review letters* 110, 196002.
- Reese, S., Govindjee, S., 1998. A theory of finite viscoelasticity and numerical aspects. *International journal of solids and structures* 35, 3455-3482.
- Shankar, R., Ghosh, T.K., Spontak, R.J., 2007. Electroactive nanostructured polymers as tunable actuators. *Advanced Materials* 19, 2218-2223.
- Sheng, J., Chen, H., Li, B., Wang, Y., 2014. Nonlinear dynamic characteristics of a dielectric elastomer membrane undergoing in-plane deformation. *Smart Materials and Structures* 23, 045010.
- Shian, S., Huang, J., Zhu, S., Clarke, D.R., 2014. Optimizing the electrical energy conversion cycle of dielectric elastomer generators. *Advanced Materials* 26, 6617-6621.

- Straube, E., Urban, V., Pyckhout-Hintzen, W., Richter, D., Glinka, C., 1995. Small-angle neutron scattering investigation of topological constraints and tube deformation in networks. *Physical review letters* 74, 4464.
- Suo, Z., 2010. Theory of dielectric elastomers. *Acta Mechanica Solida Sinica* 23, 549-578.
- Suo, Z., Zhao, X., Greene, W.H., 2008. A nonlinear field theory of deformable dielectrics. *Journal of the Mechanics and Physics of Solids* 56, 467-486.
- Suo, Z., Zhu, J., 2009. Dielectric elastomers of interpenetrating networks. *Applied Physics Letters* 95, 232909.
- Wang, H., Lei, M., Cai, S., 2013. Viscoelastic deformation of a dielectric elastomer membrane subject to electromechanical loads. *Journal of Applied Physics* 113, 213508.
- Wang, S., Decker, M., Henann, D.L., Chester, S.A., 2016. Modeling of dielectric viscoelastomers with application to electromechanical instabilities. *Journal of the Mechanics and Physics of Solids* 95, 213-229.
- Wissler, M., Mazza, E., 2005. Modeling and simulation of dielectric elastomer actuators. *Smart Materials and structures* 14, 1396.
- Yang, E., Frecker, M., Mockensturm, E., 2005. Viscoelastic model of dielectric elastomer membranes, *Smart Structures and Materials 2005: Electroactive Polymer Actuators and Devices (EAPAD)*. International Society for Optics and Photonics, 82-94.
- Yong, H., He, X., Zhou, Y., 2011. Dynamics of a thick-walled dielectric elastomer spherical shell. *International Journal of Engineering Science* 49, 792-800.
- Zhang, J., Chen, H., Li, B., McCoul, D., Pei, Q., 2015a. Coupled nonlinear oscillation and stability evolution of viscoelastic dielectric elastomers. *Soft Matter* 11, 7483-7493.
- Zhang, J., Tang, L., Li, B., Wang, Y., Chen, H., 2015b. Modeling of the dynamic characteristic of viscoelastic dielectric elastomer actuators subject to different conditions of mechanical load. *Journal of Applied Physics* 117, 084902.
- Zhang, Q., Bharti, V., Zhao, X., 1998. Giant electrostriction and relaxor ferroelectric behavior in electron-irradiated poly (vinylidene fluoride-trifluoroethylene) copolymer. *Science* 280, 2101-2104.
- Zhao, X., Hong, W., Suo, Z., 2007. Electromechanical hysteresis and coexistent states in dielectric elastomers. *Physical review B* 76, 134113.
- Zhao, X., Suo, Z., 2008. Method to analyze programmable deformation of dielectric elastomer layers. *Applied Physics Letters* 93, 251902.

- Zhao, X., Suo, Z., 2010. Theory of dielectric elastomers capable of giant deformation of actuation. *Physical review letters* 104, 178302.
- Zhou, J., Jiang, L., Khayat, R.E., 2013. Failure analysis of a dielectric elastomer plate actuator considering boundary constraints. *Journal of Intelligent Material Systems and Structures* 24, 1667-1674.
- Zhou, J., Jiang, L., Khayat, R.E., 2014. Viscoelastic effects on frequency tuning of a dielectric elastomer membrane resonator. *Journal of Applied Physics* 115, 124106.
- Zhou, J., Jiang, L., Khayat, R.E., 2015. Investigation on the performance of a viscoelastic dielectric elastomer membrane generator. *Soft Matter* 11, 2983-2992.
- Zhou, J., Jiang, L., Khayat, R.E., 2016. Dynamic analysis of a tunable viscoelastic dielectric elastomer oscillator under external excitation. *Smart Materials and Structures* 25, 025005.
- Zhou, J., Jiang, L., Khayat, R.E., 2017. Methods to improve harvested energy and conversion efficiency of viscoelastic dielectric elastomer generators. *Journal of Applied Physics* 121, 184102.
- Zhou, J., Jiang, L., Khayat, R.E., 2018. A micro–macro constitutive model for finite-deformation viscoelasticity of elastomers with nonlinear viscosity. *Journal of the Mechanics and Physics of Solids* 110, 137-154.
- Zhu, J., Cai, S., Suo, Z., 2010. Nonlinear oscillation of a dielectric elastomer balloon. *Polymer International* 59, 378-383.

## Curriculum Vitae

**Name:** Yuanping Li

**Post-secondary Education and Degrees:** University of Windsor  
Windsor, Ontario, Canada  
2013-2017 Bachelor of Applied Science

Western University  
London, Ontario, Canada  
2017-2019 Master of Engineering Science

**Honours and Awards:** Western Graduate Research Scholarship  
2017-2019

**Related Work Experience:** Teaching Assistant/Research Assistant  
Western University  
2017-2019